August 2016

Analysis of the Run-to-Run Variability Within the NAMm Forecasts for the Northeast U.S. Blizzard of 8-9 February 2013

Kaitlyn Heinlein
University of Wisconsin-Milwaukee

ANALYSIS OF THE RUN-TO-RUN VARIABILITY WITHIN THE NAM FORECASTS FOR THE NORTHEAST U.S. BLIZZARD OF 8-9 FEBRUARY 2013

by

Kaitlyn Heinlein

A Thesis Submitted in

Partial Fulfillment of the

Requirements for the Degree of

Master of Science

in Mathematics

at

The University of Wisconsin-Milwaukee

August 2016

ABSTRACT

ANALYSIS OF THE RUN-TO-RUN VARIABILITY WITHIN THE NAM FORECASTS FOR THE NORTHEAST U.S. BLIZZARD OF 8-9 FEBRUARY 2013

by

Kaitlyn Heinlein

The University of Wisconsin-Milwaukee, 2016
Under the Supervision of Professor Paul Roebber

On 8-9 February 2013, a strong extratropical cyclone brought historic winter storm conditions to the Northeast United States with a swath of one to three feet of snow falling across much of New England, with isolated pockets exceeding three feet across south-central Connecticut. Given the high socioeconomic impact that resulted from this blizzard, this study focuses on the run-to-run variability in operational model (North American Mesoscale model; NAM) forecasts leading up to the event. These forecasts, initialized forty-eight hours or less from the start of the event, showed two instances indicating a substantial shift in the expected impact. The first occurred between the runs of 0600 UTC and 1200 UTC 7 February 2013 and the second between 0000 UTC and 0600 UTC 8 February 2013. These shifts were discovered to have primarily resulted from large differences in the forecast strength of the warm air advection and the accumulated effects of those differences over time. Analysis of the mesoscale patterns show that the typical mesoscale snowband ingredients of mid-level frontogenesis and conditional symmetric instability (CSI) were not significant contributors to this high-impact case. Instead, strong and focused warm air advection, with a secondary contribution from cyclonic vorticity advection through the Sutcliffe self-development process, appears to be the main source of

cyclone track variations and the attendant intense, localized vertical motion that lead to the development of the snowbands.

TABLE OF CONTENTS

LIST OF FIGURES

I. INTRODUCTION

Snow, one of the most common forms of winter weather across the northeast United States, can cause major societal impacts, especially when it falls at a rapid rate or in large quantities. The source of such increased precipitation during the cold season can be attributed to the development of mesoscale snowbands within the comma head of extratropical cyclones over the northeast U.S. (Nicosia and Grumm 1999; Novak et al. 2004). Since snowfall resulting from mesoscale bands can be substantial over a short period of time, it can often cause near whiteout conditions in localized areas, affecting both ground and air travel, while also potentially causing numerous power outages and sometimes even death. Therefore, accurate forecasts of mesoscale snowbands are important to reduce such impacts in the future; however, one of the most pertinent challenges related to snowband forecasting is the considerable amount of uncertainty that lies within the temporal and spatial occurrence of band formation and evolution (Novak and Colle 2012).

There have been numerous studies which have examined the environments for which mesoscale snowbands develop and evolve in. Results from these studies, including that of Nicosia and Grumm (1999), Jurewicz and Evans (2004), Novak et al. (2004, 2006, 2010), have established the collocation of three distinctive ingredients to characteristically be present within such environments. These three ingredients are subset to the well-known ingredients needed for deep-convection: lift, moisture, and instability (Schultz and Schumacher 1999). In particular, the source of lift typically attributed to mesoscale snowband development within the "comma head" portion, or the northwest side of the surface cyclone, is that of strong mid-level frontogenesis (Novak 2004).

The second ingredient needed for development of mesoscale snowbands, and essentially for any precipitation in general, is that of sufficient moisture (usually 80% or more). Typically for mesoscale snowbands, convection that transpires is most often slantwise (Jurewicz and Evans 2004; Novak et al. 2006). This type of convection occurs when parcels are stable to vertical and horizontal motions but unstable to slantwise motions. In order for a parcel to be lifted slantwise, saturation must be present so that the instability, the third necessary ingredient, may be released (Shultz and Schumacher 1999). Particularly for slantwise convection, conditional symmetric instability (CSI), a specific type of moist symmetric instability (MSI), is most often released because in order for air parcels to be unstable to slantwise motions, the saturation must be present, thus making MSI "conditional" (Shultz and Schumacher 1999). Overall, it is important that these three ingredients: strong mid-level frontogenesis, sufficient moisture, and conditional symmetric instability, are collocated in order for mesoscale snowbands to develop and continually evolve within an extratropical cyclone.

Through various climatologies and case studies, these three main ingredients have been comprehensively explored. Nicosia and Grumm (1999) examined three snowstorms which affected the northeastern U.S. with intense mesoscale snowbands and found that forecasters can anticipate regions for snowband development if strong mid-level frontogenesis coincides with a deep layer of negative equivalent potential vorticity (EPV). Within the study, the negative EPV was most often associated with the release of CSI after reaching a layer of saturation. Novak (2004) on the other hand examined 75 northeastern U.S. snowfall cases in which banding occurred within the comma head portion of the cyclone. Of those cases the most frequent type of banding observed was that of single banded events. Thus, upon investigating a few case studies in which this type of single banding occurred, it was suggested that deep layer frontogenesis enhanced by temperatures advections, in the presence of moist symmetric stability reduced by

differential moisture advections, was key in the forcing and maintenance of banded structure. These results were corroborated within the study conducted by Jurewicz and Evans (2004) in which two differing synoptic situations produced diverse mesoscale snowbands. However, regardless of the shape, intensity, or size of the bands, both situations exemplified that the presence and collocation of strong mid-level frontogenesis and reduced stability is likely attributed to banded occurrence.

With the established basis that mesoscale snowbands likely result from the three main ingredients discussed above, Novak et al. (2006) developed a forecast strategy for northeast U.S. cyclones in which these ingredients were assessed at different time frames leading up to snowband events. Through application of this strategy to a specific snowstorm, it was proven that evaluation of these ingredients can lead to accurate forecasts of snowband development and subsequent evolution. Evans and Jurewicz (2009) added to the overall forecast strategy by indicating that the three main snowband ingredients should be closely examined in terms of their magnitude, depth, and persistence in order to better determine the total snowfall amount for a given event. Specifically, for this study the North American Mesoscale Forecast System (NAM) was used and results illustrated that forecasts surpassing twelve hours became increasingly less reliable, as the correlations between the snowfall and the forecast banded ingredients decreased likely due to spatial and temporal displacements of the banded structures. This hypothesis was confirmed by Novak and Colle (2012) who through use of a multi-model ensemble explored the predictability of the three northeastern U.S. snowfall events in which banding occurred to find that uncertainty lies not only within the occurrence of snowbands, but also within the location and timing of their evolution, even at forecast projections less than twenty-four hours.

In order to better understand the run-to-run variability in snowband occurrence, timing, and location, the goal of this study is to assess the meteorological conditions, especially the three

main snowband ingredients, in which a strong extratropical cyclone such as the event which occurred on 8-9 February 2013 produced major winter storm conditions across the northeast U.S. Given the intense mesoscale snowbands that developed within this particular event, impacts were quite severe, as numerous flight cancelations, travel bans, prolonged regional power outages, and even some fatalities occurred (NWA 2014; Associated Press 2014). Diagnosing the variability that occurred within the modeled forecasts of this particular event may provide some insight for future mesoscale model development alongside proposing potential improvements for current operational forecast strategies.

II. OVERVIEW AND METHODOLOGY

a. Case Overview of 8-9 February 2013

Before major winter storm conditions were underway, the 8-9 February 2013 event started out as two distinct upper-level waves moving across the United States. Referring to the upper-level analysis data from the NCAR MMM online image archive, 500 hPa analyses from 0000 UTC 7 February exhibit a shortwave over the Intermountain West with a secondary wave over eastern Texas (Fig. 1a). These waves progressed eastward over time, with the northern wave stretching across much of the Northern Plains by 1200 UTC 7 February, while the southern one becomes located over the Gulf Coast region (Fig. 1b). Within the next analysis time frame, 0000 UTC 8 February (Fig. 1c), the waves become slightly more defined, especially the southern one, with the axis of the northern wave running through the Midwest, while the southern wave is seen over South Carolina. By 1200 UTC 8 February, these waves become noticeably stronger and are also found in closer proximity, as the northern wave runs through the central Great Lakes Region and into the Ohio Valley, while the southern wave continues to progress up the East Coast and becomes located across Virginia and North Carolina (Fig. 1d). The merging of these two waves over the Northeast U.S. is then evident within the 0000 UTC 9 February analysis (Fig. 1e), with the phasing appearing to have been completed shortly after considering the 1200 UTC 9 February analysis (Fig. 1f) depicts one deep trough exiting off to the northeast as the event slowly comes to an end.

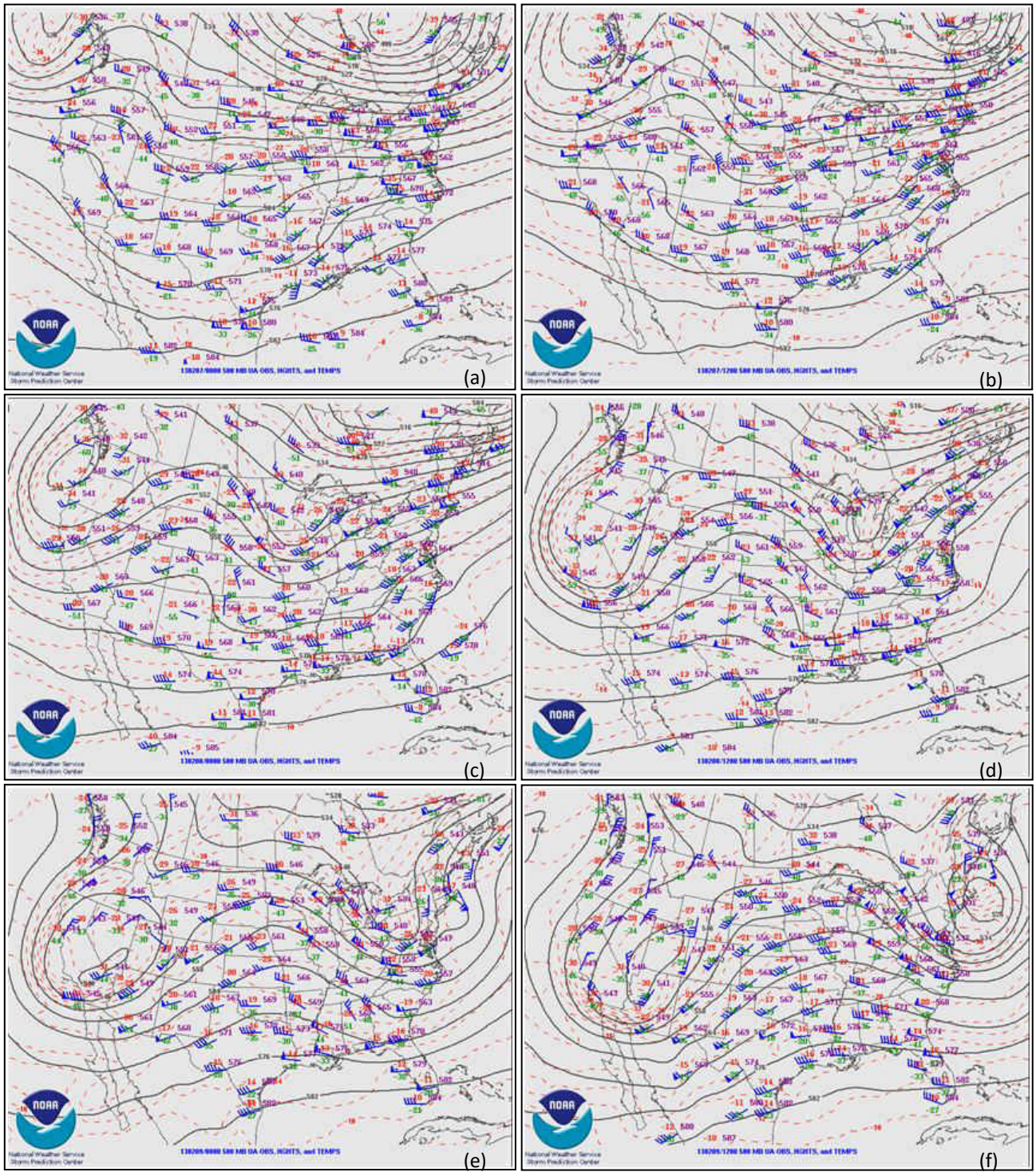

Fig. 1. (a)-(f) Storm Prediction Center 500 hPa Analyses valid at (a) 0000 UTC 7 Feb, (b) 1200 UTC 7 Feb, (c) 0000 UTC 8 Feb, (d) 1200 UTC 8 Feb, (e) 0000 UTC 9 Feb, (f) 1200 UTC 9 Feb 2013.

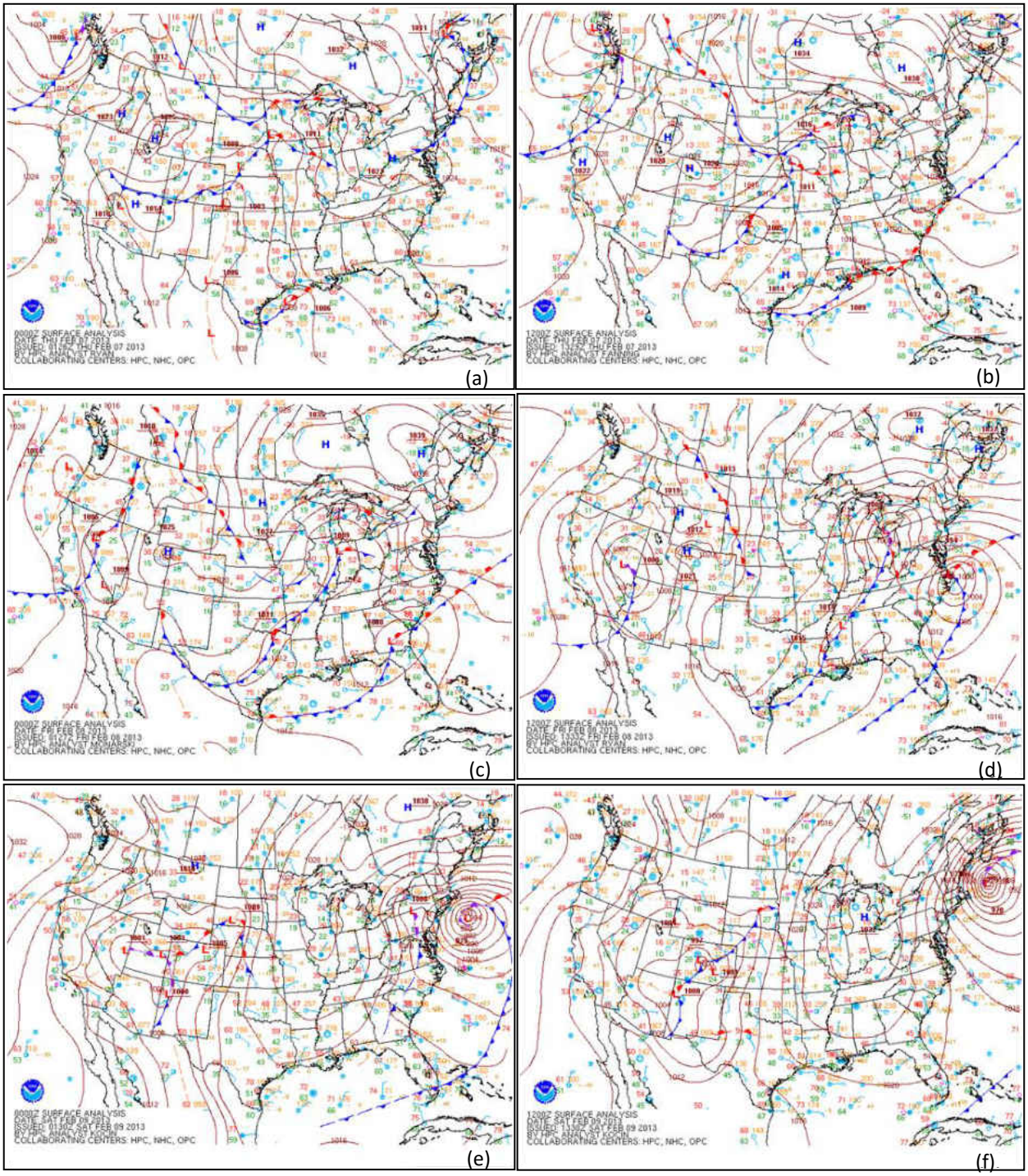

Fig. 2. (a)-(f) Weather Prediction Center Surface Analyses valid at (a) 0000 UTC 7 Feb, (b) 1200 UTC 7 Feb, (c) 0000 UTC 8 Feb, (d) 1200 UTC 8 Feb, (e) 0000 UTC 9 Feb, (f) 1200 UTC 9 Feb 2013.

Meanwhile, at the surface throughout this time period, two areas of low pressure develop, with one apparent across Iowa at 1200 UTC 7 February, while another starts to strengthen over the central Gulf Coast (Fig. 2b). The weaker, northern system progresses eastward over time, sliding south of the Great Lakes, while the southern system begins to take a typical Nor'easter path, as it begins to move across Florida/Georgia before heading up the coast (Fig. 2c). By 1200 UTC 8 February, the northern cyclone is positioned over Lake Erie having central pressure near 1008 hPa, while the southern one is located off the North Carolina coast at 1000 hPa (Fig. 2d). Both cyclones continue to generate their own individual precipitation with the northern system, enhanced by upper-level jet divergence, bringing snowfall across the Great Lakes region, while the southern system has strong lower-level lift to support its precipitation that is now starting to transition from rain to a frozen mix. This occurs along the northern periphery of its precipitation shield at this time, as a large anticyclone across eastern Canada has enforced cold air at the surface across the Northeast. Thus, as the cyclone propagates northeastward, precipitation along its northern edge will start to fall through a column in which cold air near the surface will cause for a majority of the precipitation to freeze.

From this point on over the next 24 hours (Figs. 1e,f), the northern and southern streams begin to merge as the troughs near closer to one another and coupling of their upper-level jet entrance/exit regions occurs. With the phasing of the vorticity from each trough, strong differential cyclonic vorticity advection will begin to enhance the trough-ridge structure, which too will augment the baroclinicity overall (Gaza and Bozart 1990). Thus, this phasing of the two streams leads to the extratropical cyclone along the coast intensifying and undergoing rapid cyclogenesis (Figs. 2d-f). All the while, the precipitation associated with each system begins to phase together as well, with intense precipitation occurring across the Northeast U.S. More specifically, across the New England area, strong banded precipitation begins to form across

Long Island around 0000 UTC 9 February (Fig. 3), with reflectivity values in excess of 55 dBZ as mixed precipitation and heavy snow is experienced. Over the next six to twelve hours, the banded structure remained evident as it pivoted across the New England region (Figs. 4a-d), but reflectivity values fell more to a range of 25-40 dBZ as the hydrometeor type became more consistent, thus indicating a transition to mostly snow (Picca et al. 2014). Nonetheless, this range is typical for snowbands (Novak 2004), and with the strong east/northeasterly winds occurring simultaneously, as the central pressure of the system continually deepened toward 976 hPa, blizzard conditions were experienced across New England during this time frame. Not until around 1200 UTC 9 February did the snowfall start to decrease as the system lifted off to the northeast with snow ending around 1800 UTC 9 February.

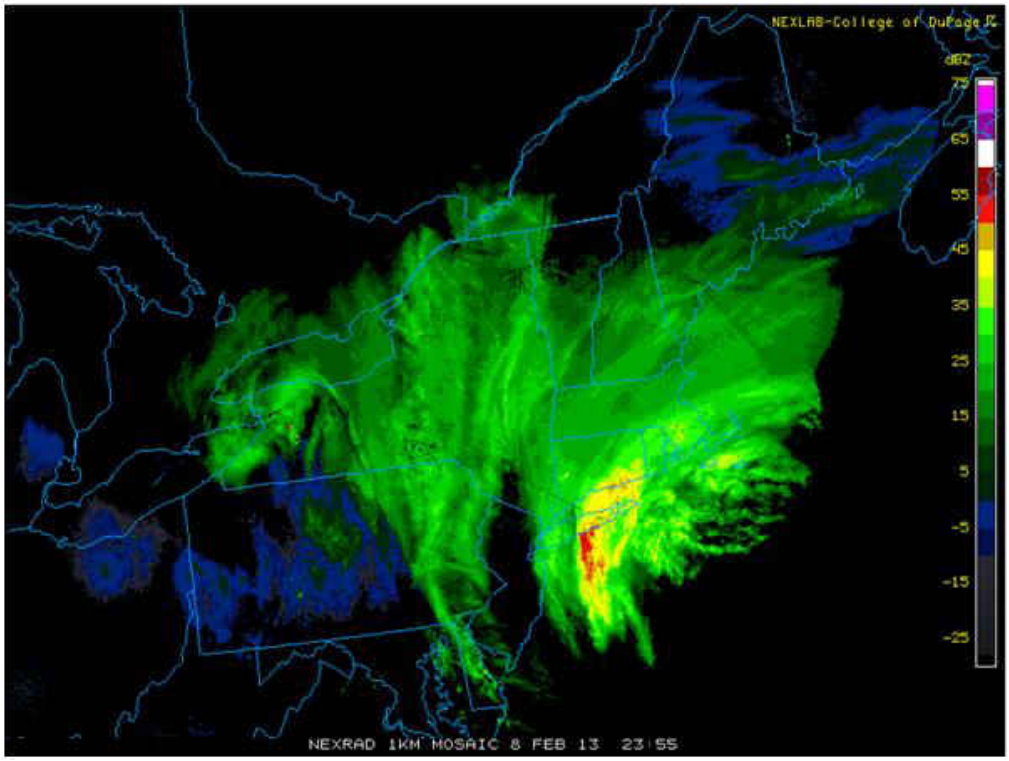

Fig. 3. Regional mosaic of radar reflectivity at 2355 UTC 8 February 2013.

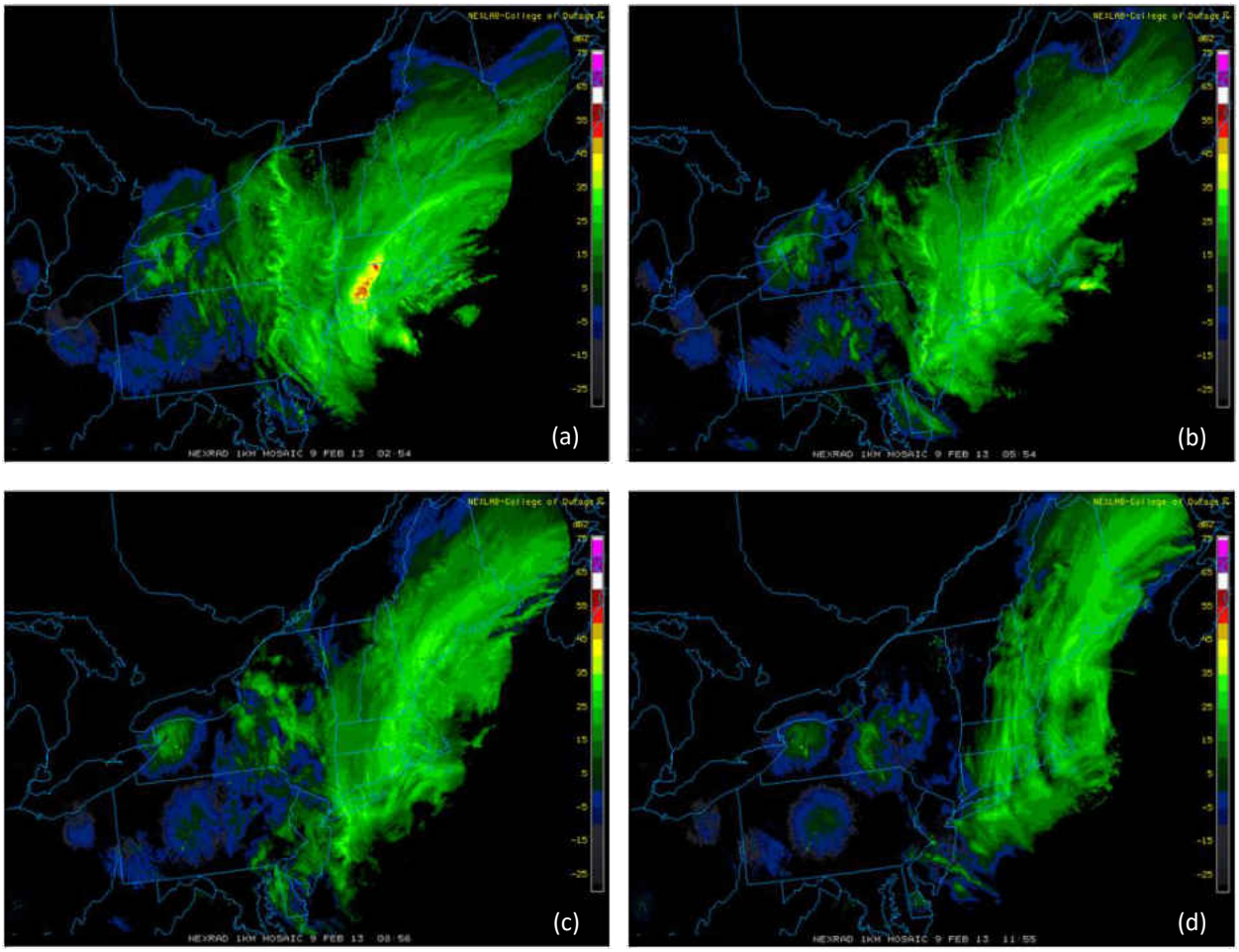

Fig. 4. (a)-(d) Regional mosaic of radar reflectivity on 9 Feb 2013 at (a) 0254 UTC, (b) 0554 UTC, (c) 0856 UTC, (d) 1155 UTC.

Impacts from this strong winter storm included a large swath of accumulated snowfall ranging from one to three feet from northeastern New Jersey extending northeast up through the entire southeastern half of Maine. Isolated pockets of snowfall exceeded three feet across Connecticut, with 40 inches reported in Hamden, CT. Other impacts across the region included hurricane-force winds, coastal flooding, power outages, flight cancellations, and several fatalities. Given the large socioeconomic impact of this event, it is of interest to consider the forecasts leading up to it, with a view toward run-to-run variability and the effects of that on forecast utility.

b. Data & Methodology

In order to examine the 8-9 February 2013 event, two datasets were utilized. The first was NEXRAD data viewed through the NCAR MMM online image archive. This particular dataset was chosen not only for its availability online, but also because of the composite format. This was useful since snowbands often stretch across multiple radars at once, making an overview of the event more readily obtainable. Viewing these data through the Novak (2004) definition, in which a single band snowband is characterized as one that presents a 30 dBZ linear reflectivity feature with length greater than 250 km and width of 20-100 km for at least two hours, it was verified that multiple single-band snowbands occurred throughout the evolution of the event.

To examine the operational forecast model performance regarding the observed snowbands, the North American Mesoscale Forecast System (NAM) model, initialized and run every six hours (0000 UTC, 0600 UTC, 1200 UTC, 1800 UTC) by the National Centers for Environmental Prediction (NCEP), was used. This particular model, with a horizontal resolution of 12 km, was appropriate to employ for this study, as it is not only capable of capturing the type of banded structure defined by Novak (2004), but it is also widely employed within the forecasting community. The 60 vertical levels of this model configuration allow detailed examination of the mesoscale dynamics associated with the snowbands. For more information regarding the configuration of the NAM, a description file is available through NCEP's Environmental Modeling Center, the link to which is found within the References section of this thesis.

To diagnose the run-to-run variability of NAM forecasts for the 8-9 February 2013 event, forecasts were analyzed from those initialized on 0000 UTC 7 February, prior to the occurrence

of the event, and then at every run time available through 1200 UTC 9 February, when the overall precipitation started to diminish and the extratropical cyclone began to lift northeastward away from the region. Primary analysis began with viewing the evolution of the forecast reflectivity projected within each run time. Of particular interest were any shifts within the forecast reflectivity occurring between run times that would potentially lead to a change within the overall timing and/or location of heavy snowfall, or at the very least increase forecast uncertainty. This is especially important given the high population density of the northeastern United States and its proximity to the open ocean. Thus, if a significant shift is noted from one run to the next, the goal is to identify when and how these differences occurred and what their subsequent evolution is through the run.

Both synoptic and mesoscale patterns were analyzed from run-to-run. From a synoptic perspective, this required understanding of the pattern evolution largely based on quasigeostrophic dynamics (differential vorticity and the Laplacian of temperature advection). Q-Vector analyses were created by interpolating the NAM data from its native grid to a (coarser) grid of 0.5 degree by 0.5 degree to focus identification of the synoptic patterns. Low-level and mid-level total wind frontogenesis calculations are also conducted to improve understanding of mesoscale precipitation production. Along with this, the susceptibility to slantwise displacements within the environment is also assessed through the relationship of geostrophic momentum and saturation equivalent potential temperature (Mg-θ_{es}) as described by Shultz and Schumacher (1999), as it collocation with frontogenesis often times is the primary forcing for single banded precipitation (Novak 2004). Through these analyses, the overall forecast performance of the NAM and its run-to-run variability for this particular event is assessed.

III. RESULTS

a. Overview of NAM forecasts

Beginning 36 hours prior to when observed reflectivity first appeared across New England from the southern system, the NAM forecast initialized at 0000 UTC 7 February was significantly delayed and well-offshore as the surface cyclone propagated far from the coastline (Figs. 5e-h). Thus, New Jersey and the NYC metropolitan area remained dry within this particular forecast, while eastern portions of New England were forecast to receive the bulk of the heavy snow (Figs. 5a-d). Regardless of the location of the forecast reflectivity, it is important to note that this NAM run, initialized more than 48 hours out from the most intense part of the observed event, is depicting a cyclone that undergoes rapid cyclogenesis and brings heavy snow and strong winds to New England. The next run time, 0600 UTC 7 February, is similar, though the timing is slightly improved. Overall the depiction is the same, that of a deep cyclone propagating northeastward and producing major winter storm conditions mainly across eastern New England (Figs. 6a-h).

The first significant forecast change comes with the next run, initialized at 1200 UTC 7 February, approximately 36 hours ahead of the event. A detailed view regarding the overall synoptic and mesoscale evolution of this run compared to the previous run can be found in Part B of this section. However, this run is considerably different in that the forecast reflectivity is shifted much farther westward (Figs. 7a-d), as the surface cyclone is now forecast to stay closer to the coast (Figs. 7e-h). In this forecast, New Jersey receives considerable precipitation, while NYC sees reflectivity exceeding 40 dBZ. This change places forecasters in a difficult position given the timing, as high-impact decisions for the NYC metro area would need to be made soon.

However, since this run represents a substantial shift from the previous forecast, the lack of run consistency reduces forecaster confidence in the scenario and suggests caution.

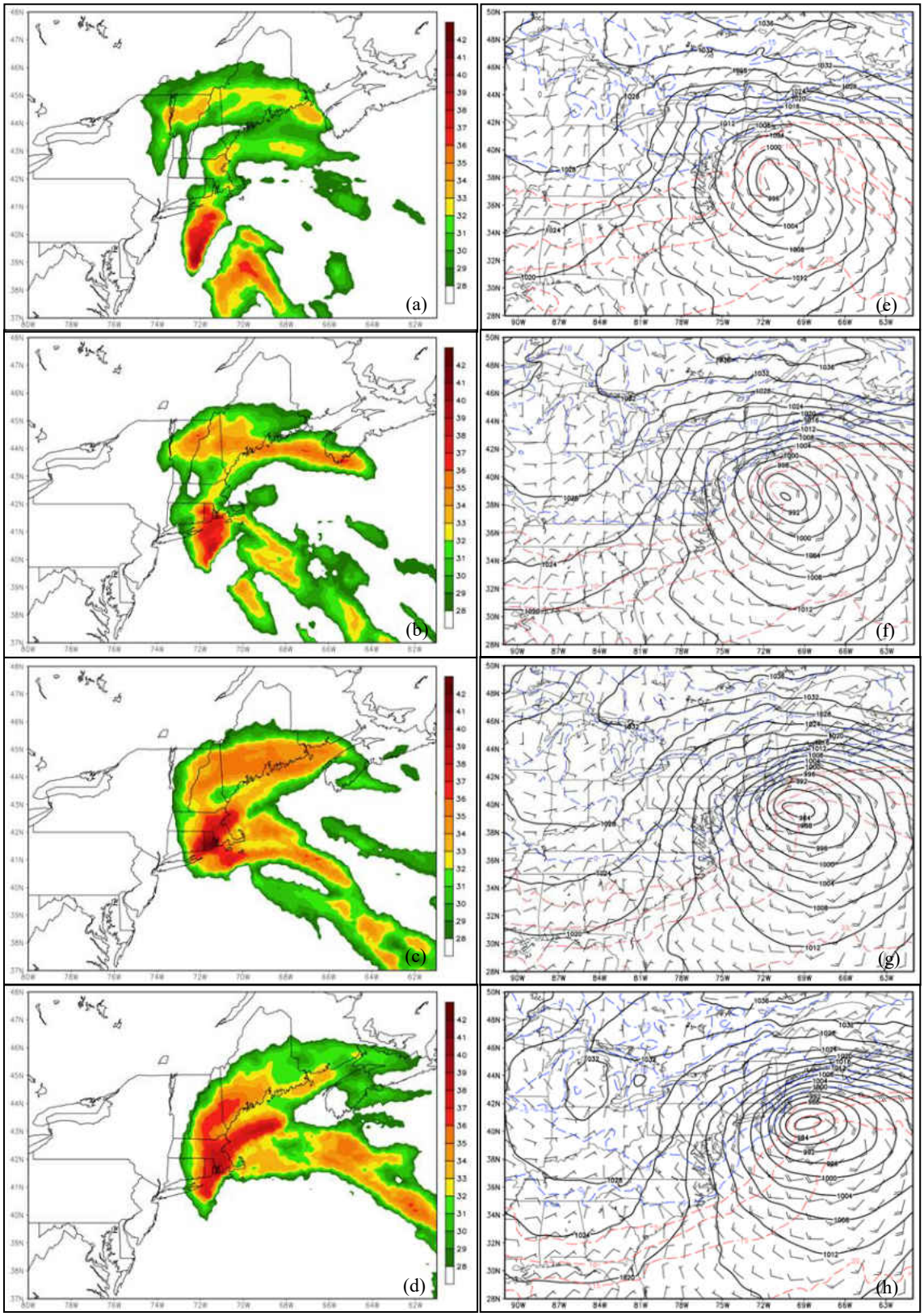

Fig. 5. 0000 UTC 7 Feb 2013 NAM forecast valid at 0300 UTC, 0600 UTC, 0900 UTC, 1200 UTC 9 Feb 2013 (top to bottom) for (a)-(d) composite reflectivity (dBZ); (e)-(h) mean sea level pressure (hPa, solid), 1000 hPa temperature (C, dashed), and 1000 hPa winds (m/s, barb).

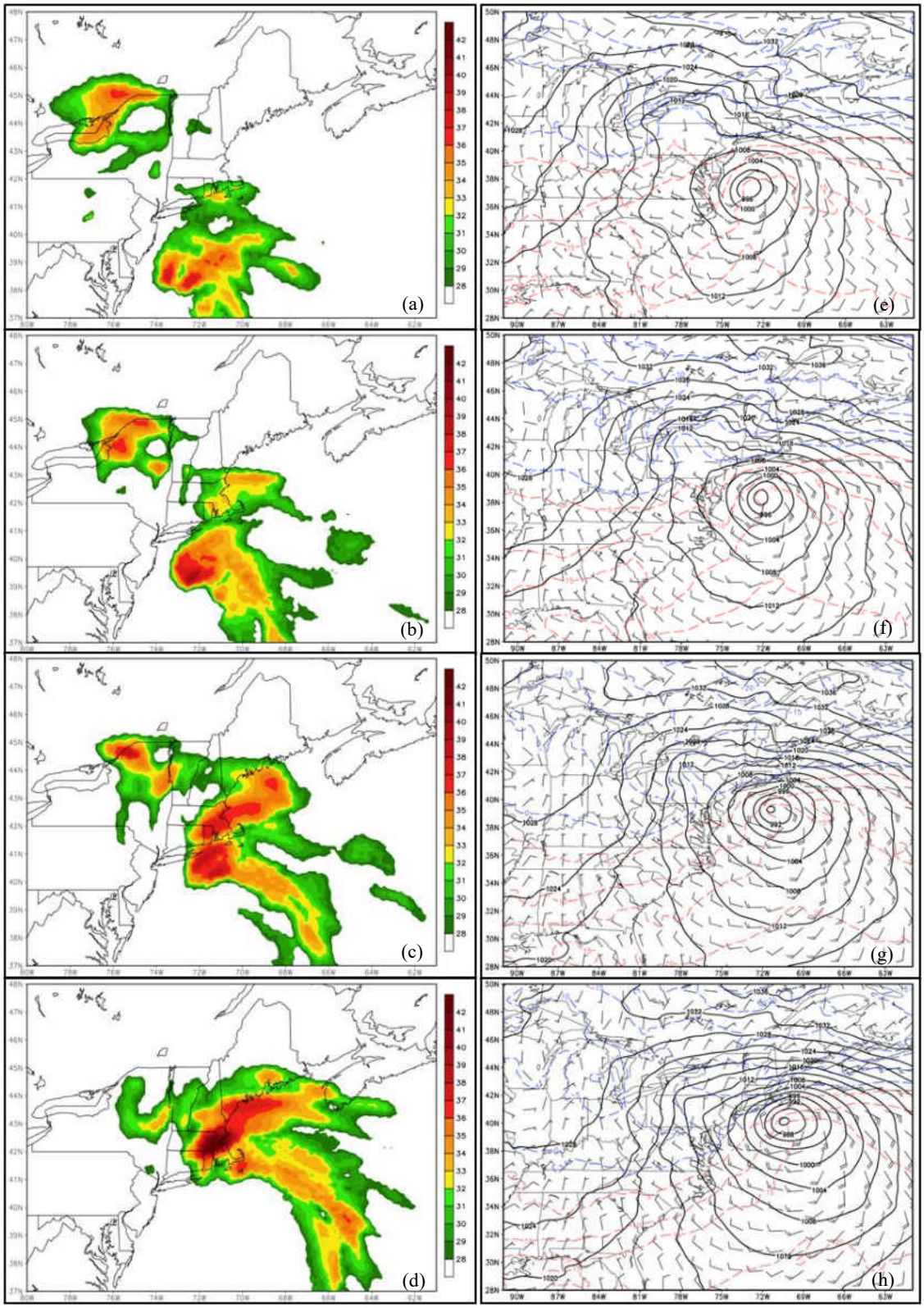

Fig. 6. 0600 UTC 7 Feb 2013 NAM forecast valid at 2100 UTC 8 Feb 2013 and 0000 UTC, 0300 UTC, 0600 UTC 9 Feb 2013 (top to bottom) for (a)-(d) composite reflectivity (dBZ); (e)-(h) mean sea level pressure (hPa, solid), 1000 hPa temperature (C, dashed), and 1000 hPa winds (m/s, barb).

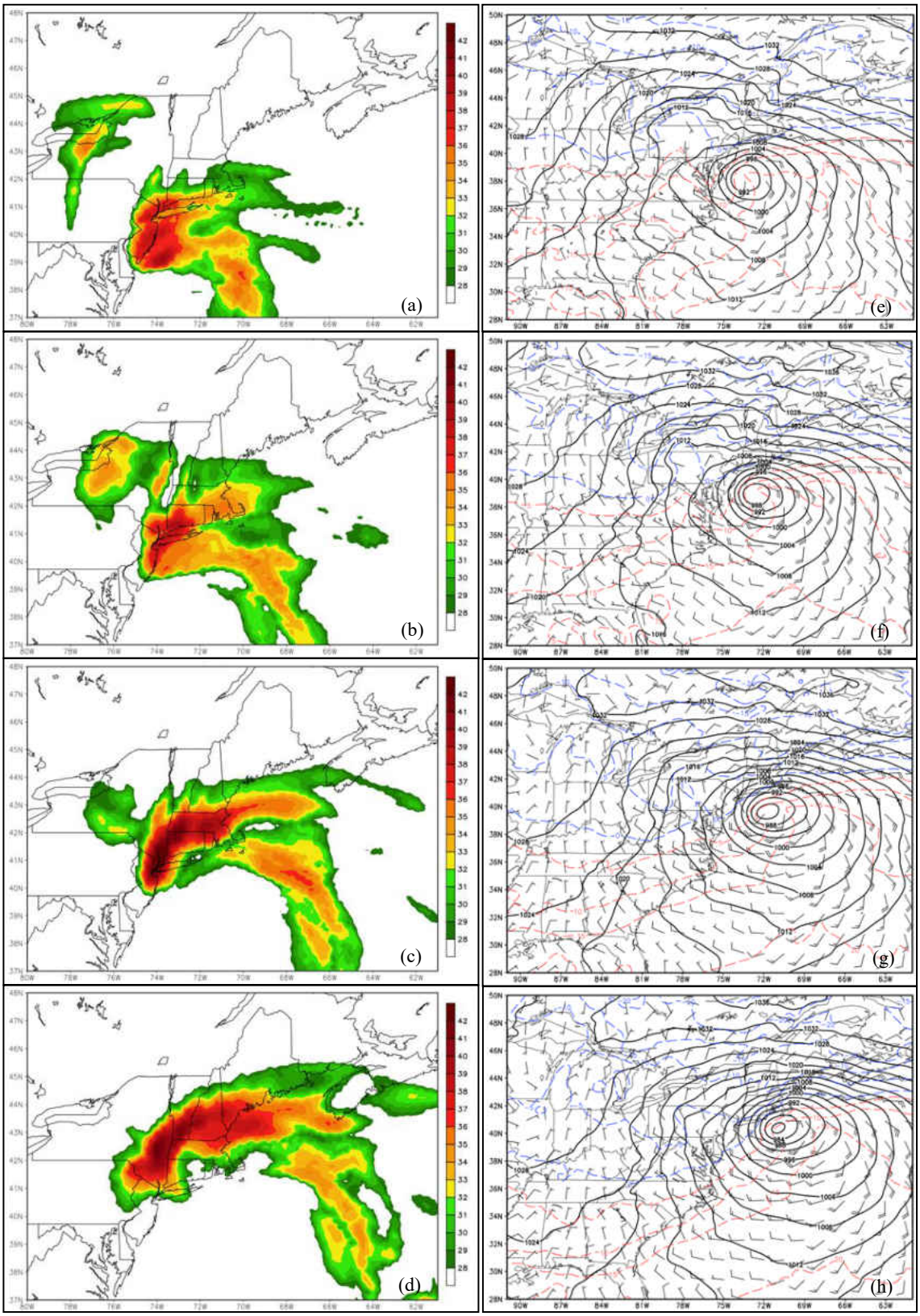

Fig. 7. 1200 UTC 7 Feb 2013 NAM forecast valid at 2100 UTC 8 Feb 2013 and 0000 UTC, 0300 UTC, 0600 UTC 9 Feb 2013 (top to bottom) for (a)-(d) composite reflectivity (dBZ); (e)-(h) mean sea level pressure (hPa, solid), 1000 hPa temperature (C, dashed), and 1000 hPa winds (m/s, barb).

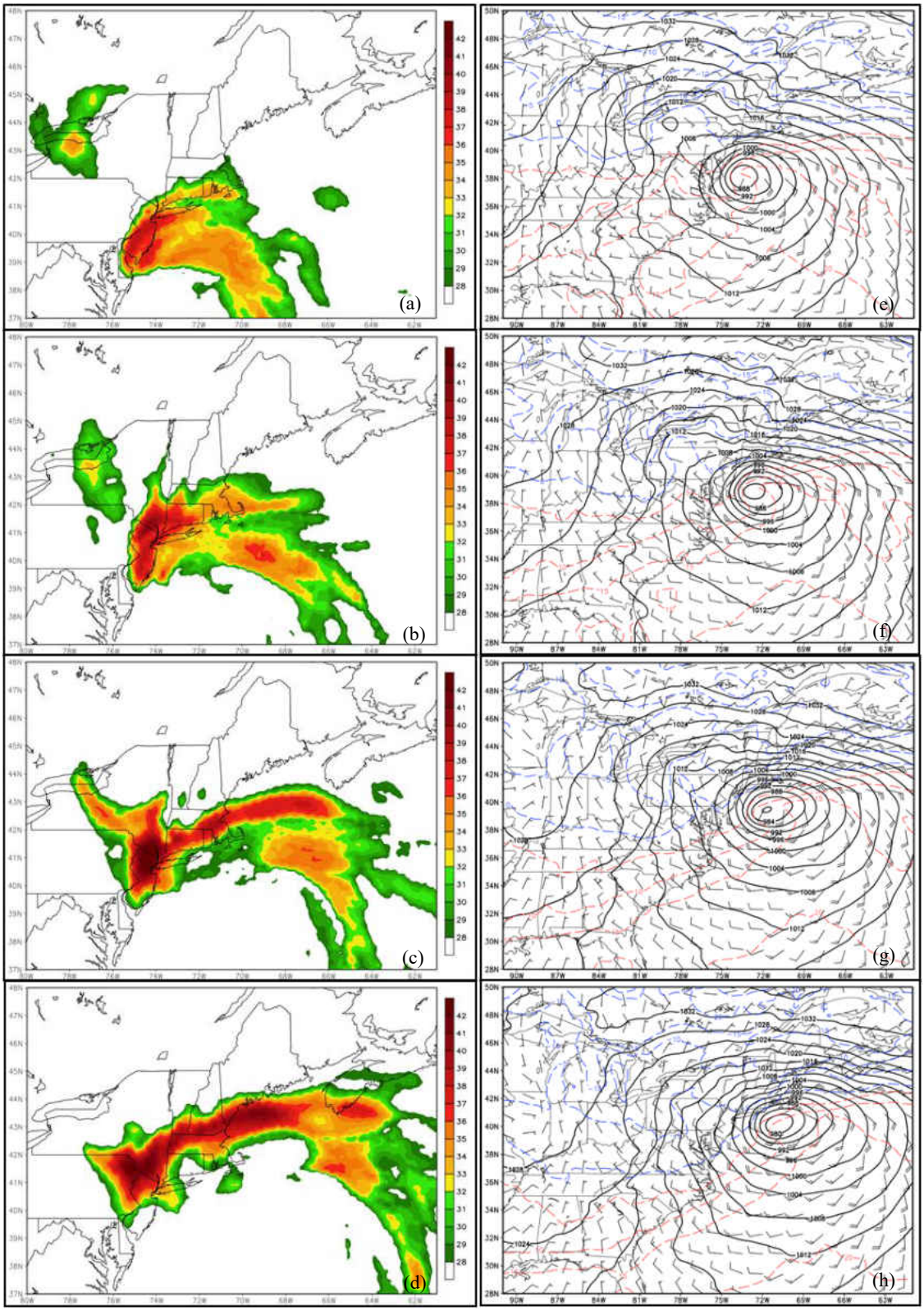

Fig. 8. 0000 UTC 8 Feb 2013 NAM forecast valid at 2100 UTC 8 Feb 2013 and 0000 UTC, 0300 UTC, 0600 UTC 9 Feb 2013 (top to bottom) for (a)-(d) composite reflectivity (dBZ); (e)-(h) mean sea level pressure (hPa, solid), 1000 hPa temperature (C, dashed), and 1000 hPa winds (m/s, barb).

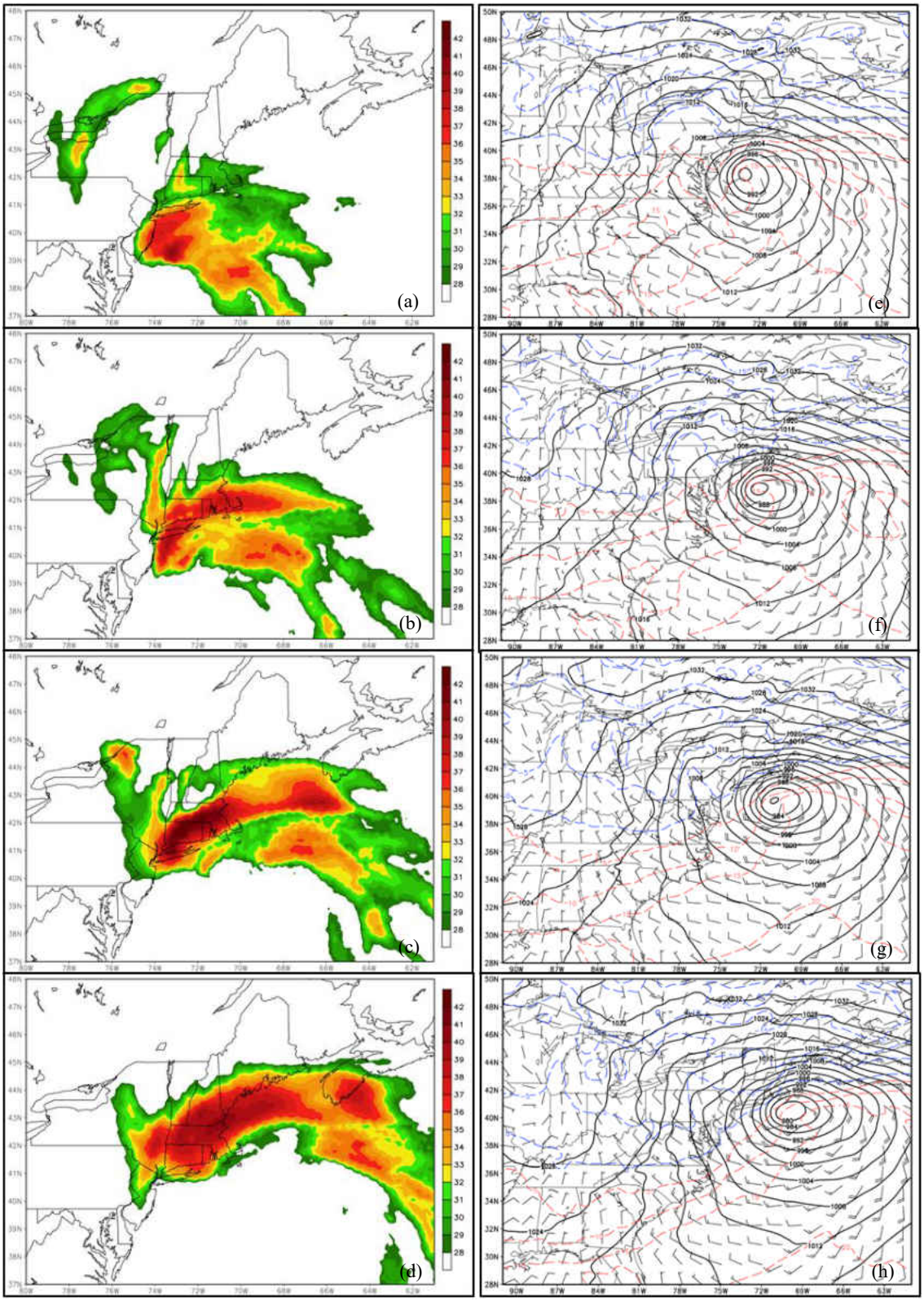

Fig. 9. 0600 UTC 8 Feb 2013 NAM forecast valid at 2100 UTC 8 Feb 2013 and 0000 UTC, 0300 UTC, 0600 UTC 9 Feb 2013 (top to bottom) for (a)-(d) composite reflectivity (dBZ); (e)-(h) mean sea level pressure (hPa, solid), 1000 hPa temperature (C, dashed), and 1000 hPa winds (m/s, barb).

The next run, initialized at 1800 UTC 7 February, largely holds to this new scenario. There are slight differences in the intensities and locations of the snowbands, but overall, New Jersey and NYC both receive persistent heavy precipitation. Generally, the same can be said for the following run from 0000 UTC 8 February (Figs. 8a-h), now only about 24 hours ahead of the event. Thus, excepting a small westward shift of reflectivity and very slight differences in timing, these three runs were self-consistent. According to Evans and Jurewicz (2009), however, the magnitude, depth, persistence, timing and location of features attributed to making such intense snowband signatures are unreliable at anything more than twelve hours out. Forecasters are then left in the position of an imminent storm that has very high-impact potential and with some internal consistency (at least in the several latest runs) regarding NYC and environs.

The next run, initialized at 0600 UTC 8 February (Figs. 9a-h), unfortunately seems to confirm the Evans and Jurewicz (2009) finding, as the reflectivity pattern shifts *significantly* to the east, focusing the heavy precipitation on Long Island and states to the north rather than New Jersey and NYC. Synoptic and mesoscale details associated with this significant shift are discussed further in Part C of this section. Following this large shift in the forecast, the subsequent run times largely hold to this new scenario.

b. Forecast shift between 0600 UTC 7 February and 1200 UTC 7 February

At 500 hPa, the 0600 UTC 7 February run and the 1200 UTC February run (hereafter referred to as 0706Z and 0712Z respectively), display similar zonal flow with a shallow, broad trough found across the Southeast U.S. valid at 1200 UTC 7 February (Figs. 10a,b). The next time frame valid at 1500 UTC 7 February, exhibits more or less the same pattern, though slightly stronger wind speeds can be seen across the Gulf Coast within 0712Z this time at both 500 hPa

(Figs. 10e,f) and 850 hPa (Figs 10g,h). Although the difference in magnitude of the winds is small (on the order of 5 m/s or less), both 0706Z and 0712Z evolve quite differently from this point on, continually building upon this small error that came about within their respective nine and three hour forecast (see below).

By the 1800 UTC 7 February valid time (Fig. 11), both the 500 hPa and 850 hPa winds have increased in the runs, yet 0712Z continues to show stronger winds across a much broader area over the Gulf Coast. At 850 hPa within 0712Z, heights have lowered over this region to form a closed 147 dam contour, while at the surface there is a 1012 hPa closed contour. For 0706Z, the lowest 850 hPa height, which is not closed off, is 150 dam, with only some inverted troughing near the surface. These differences can be traced back to variations between the magnitudes of the winds, especially those at 850 hPa. More specifically, at this time the thermal gradient is relatively north-south across the Southeast U.S., and the winds are orientated perpendicular to this gradient as they come up out of the south. Thus, both runs are producing warm air advection (WAA) at this time; however, with the winds being stronger within 0712Z, there is greater WAA occurring as compared to 0706Z. Q-Vector diagnostics confirm this, as 0712Z shows a broader area of 850 hPa Q-Vector convergence across western Georgia.

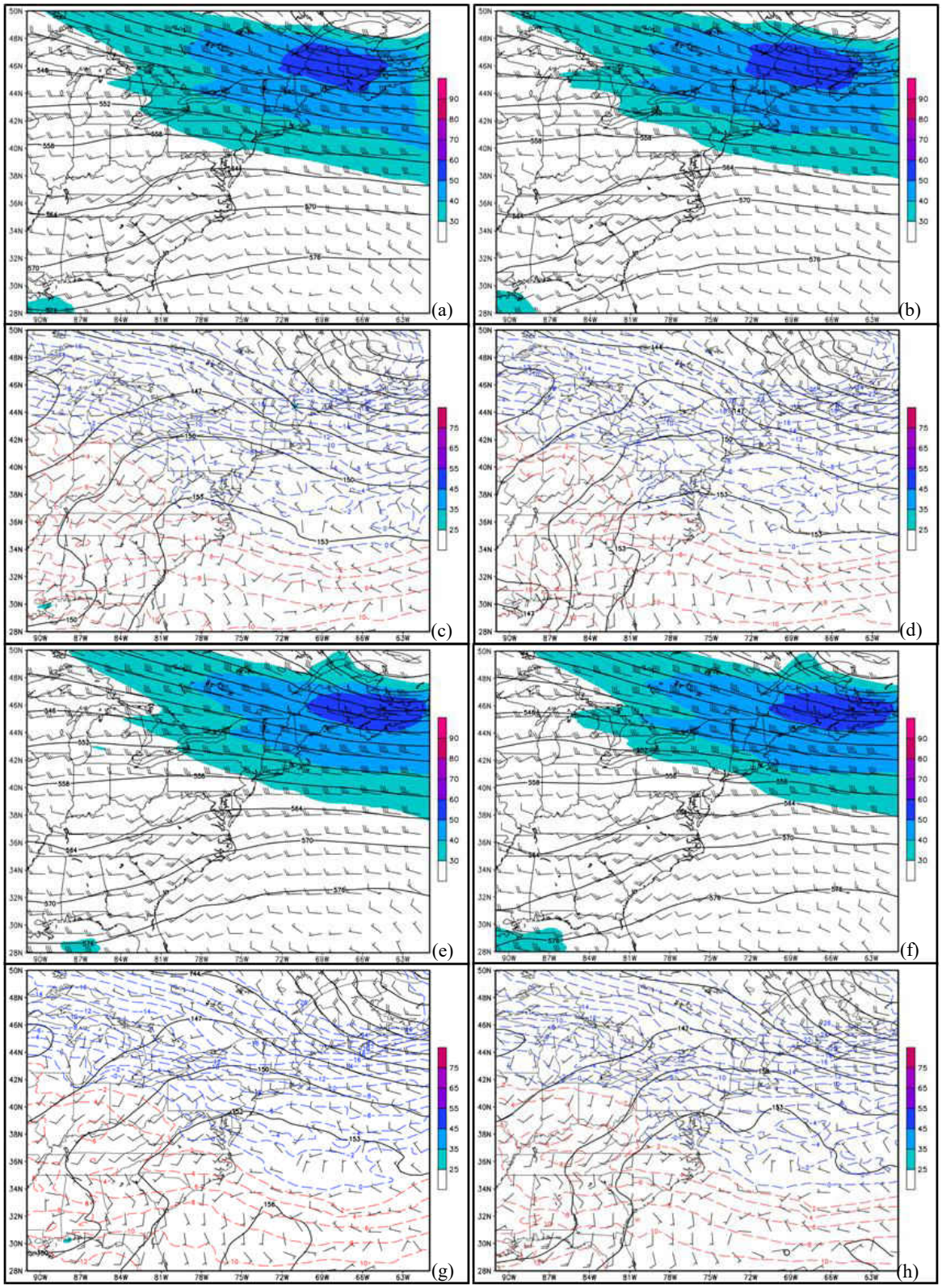

Fig. 10. 0600 UTC (left) and 1200 UTC (right) 7 Feb 2013 NAM forecasts for 500 hPa heights (dam, solid) and winds (m/s, barb) valid at (a,b) 1200 UTC 7 Feb 2013 and (e,f) 1500 UTC 7 Feb 2013; 850 hPa heights (dam, solid), temperature (C, dashed), and winds (m/s, barb) valid at (c,d) 1200 UTC 7 Feb 2013 and (g,h) 1500 UTC 7 Feb 2013.

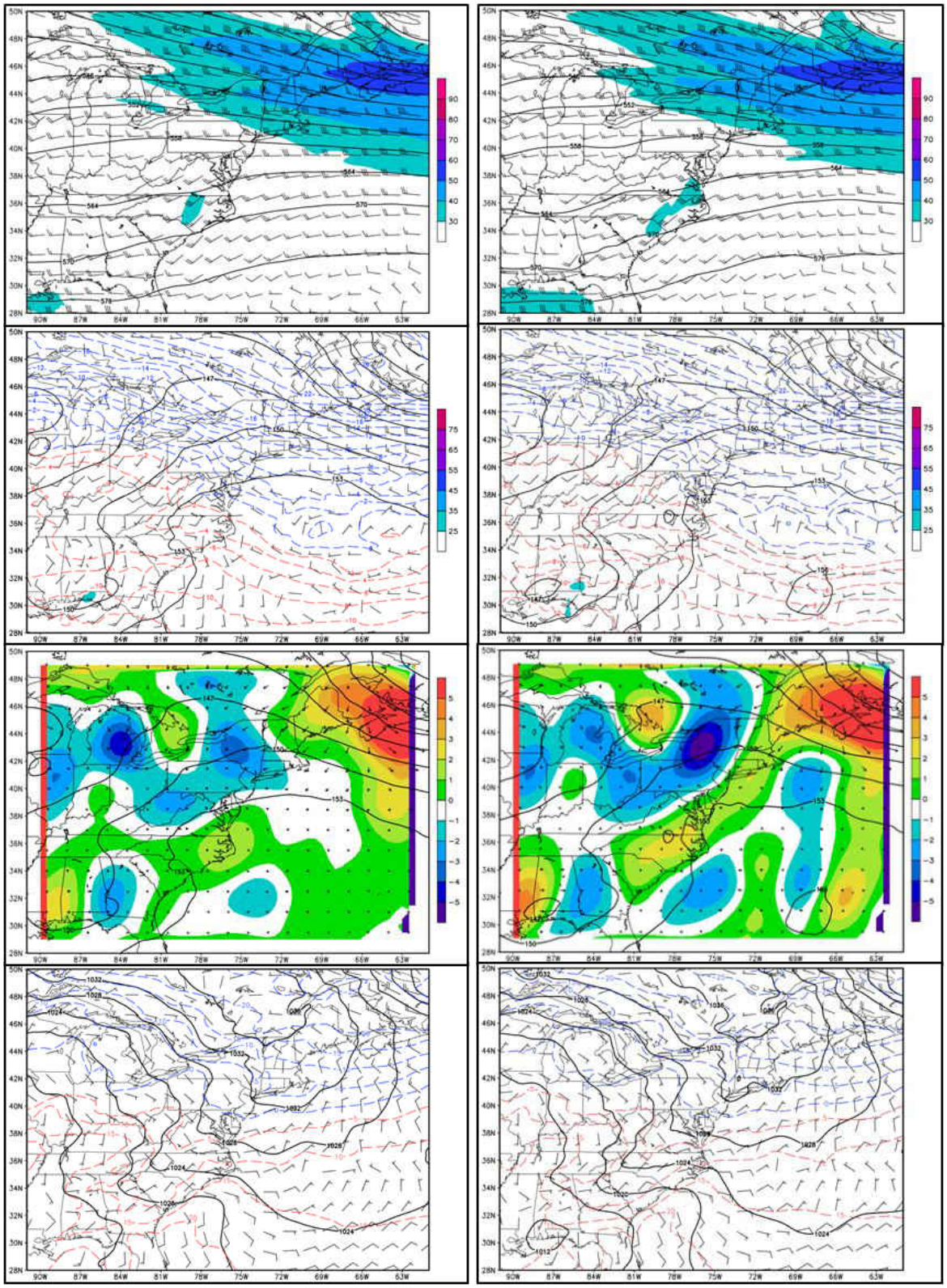

Fig. 11. 0600 UTC (left) and 1200 UTC (right) 7 Feb 2013 NAM forecasts valid at 1800 UTC 7 Feb 2013 for (top to bottom) 500 hPa heights (dam, solid) and winds (m/s, barb); 850 hPa heights (dam, solid), temperature (C, dashed), and winds (m/s, barb); 850 hPa Q-vectors (arrows in $x10^{-7}$ Pa m^{-1} s^{-1}), Q-vector divergence (10^{-12} Pa m^{-2} s^{-1}); mean sea level pressure (hPa, solid), 1000 hPa temperature (C, dashed), and 1000 hPa winds (m/s, barb).

Focusing in on the evolution of the warm air advection pattern, at 2100 UTC 7 February valid time, more 850 hPa Q-Vector convergence is evident in 0712Z compared to 0706Z (Fig. 12). Both runs exhibit a Q-Vector couplet of convergence and divergence located over eastern Georgia and southwestern Alabama respectively; however, the magnitudes of these couplets are different. 0712Z displays a stronger couplet, thus indicating that stronger WAA is occurring within this run. The Sutcliffe self-development process (Sutcliffe and Forsdyke 1950; Palmén and Newton 1969, pp 324-326; Uccelini 1990), wherein WAA ahead of the surface cyclone and beneath the upper level ridge acts to amplify (hydrostatically) the ridge and slow its progression, feeding back to stronger differential cyclonic vorticity advection and surface cyclone development, appears to be in effect.

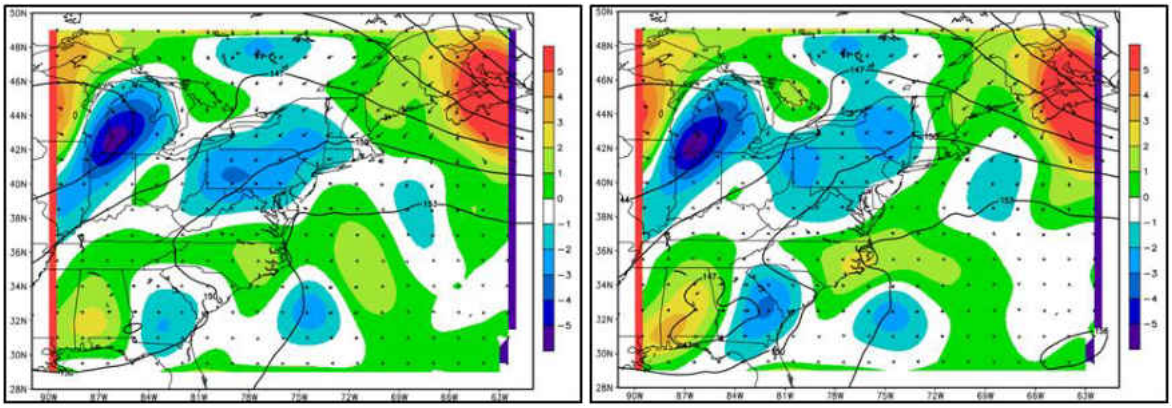

Fig. 12. 0600 UTC (left) and 1200 UTC (right) 7 Feb 2013 NAM forecasts valid at 2100 UTC 7 Feb 2013 for 850 hPa heights (dam, solid), 850 hPa Q-vectors (arrows in $x10^{-7}$ Pa m^{-1} s^{-1}), and Q-vector divergence (10^{-12} Pa m^{-2} s^{-1}).

Over the next few forecast hours (Fig. 13), this process continually builds, with noticeable ridging finally beginning to transpire around 0300 UTC 8 February and onward, especially within 0712Z. Given this amplification in the upper-level flow pattern, stronger cyclonic geostrophic vorticity advection begins to occur. This becomes evident by the valid time of 1200 UTC 8 February in which 500 hPa Q-Vector convergence is strongest over eastern portions of Virginia and North Carolina in 0712Z, while it is less prominent and located more offshore from the Mid-Atlantic Coast in 0706Z (Fig. 14). Throughout the remainder of the runs, the Q-Vector convergence remains stronger in 0712Z, allowing for the surface cyclone to deepen faster than in 0706Z, while it also remains more confined to the coast.

The tracking of the cyclone closer to the coast is attributed to the placement of the WAA. The 850 hPa Q-Vector convergence (Fig. 15) becomes stronger faster within 0712Z, while greater WAA occurs to the northeast and along the northern extent of the cyclone. This is illustrated with the couplet appearing to become more northeast-southwest orientated starting at the valid time of 1800 UTC 8 February and continuing to gradually rotate counter-clockwise before becoming almost entirely north-south orientated by 0900 UTC 9 February. However, 0706Z keeps the couplet more east-west orientated for much of the run, with it not rotating toward a northeast-southwest orientation until 0300 UTC 9 February. Through these analyses, the stronger WAA focused to the northeast and even slightly to the north of the cyclone within 0712Z allows for the surface cyclone to track closer to the coast, which is farther west than what is seen within 0706Z. Thus, the associated snowband reflectivity patterns are also shifted much further to the west throughout 0712Z.

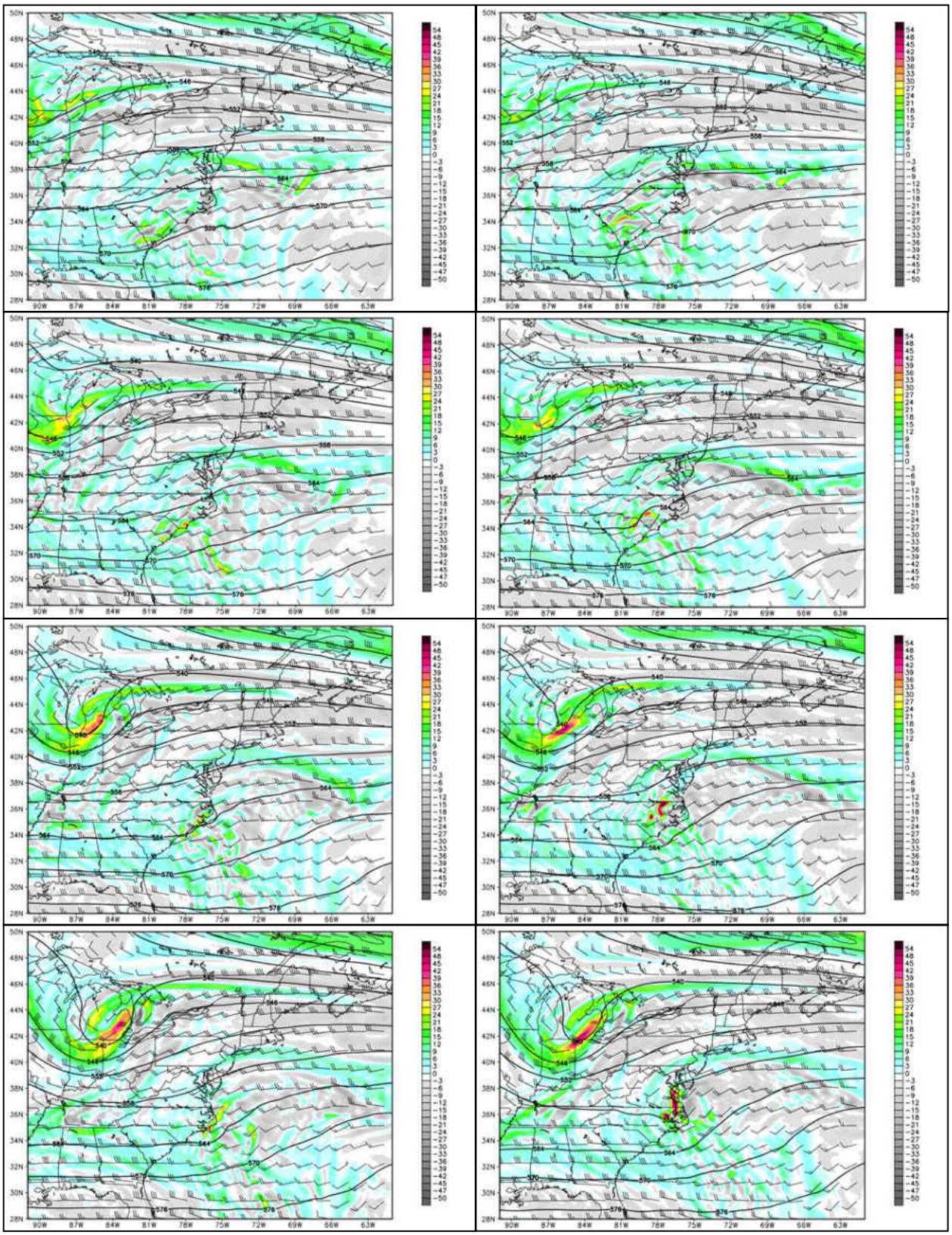

Fig. 13. 0600 UTC (left) and 1200 UTC (right) 7 Feb 2013 NAM forecasts for 500 hPa heights (dam, solid), winds (m/s, barb), and vorticity (10^{-5} s^{-1}, shaded) valid at 0300 UTC, 0600 UTC, 0900 UTC, and 1200 UTC 8 Feb 2013 (top to bottom).

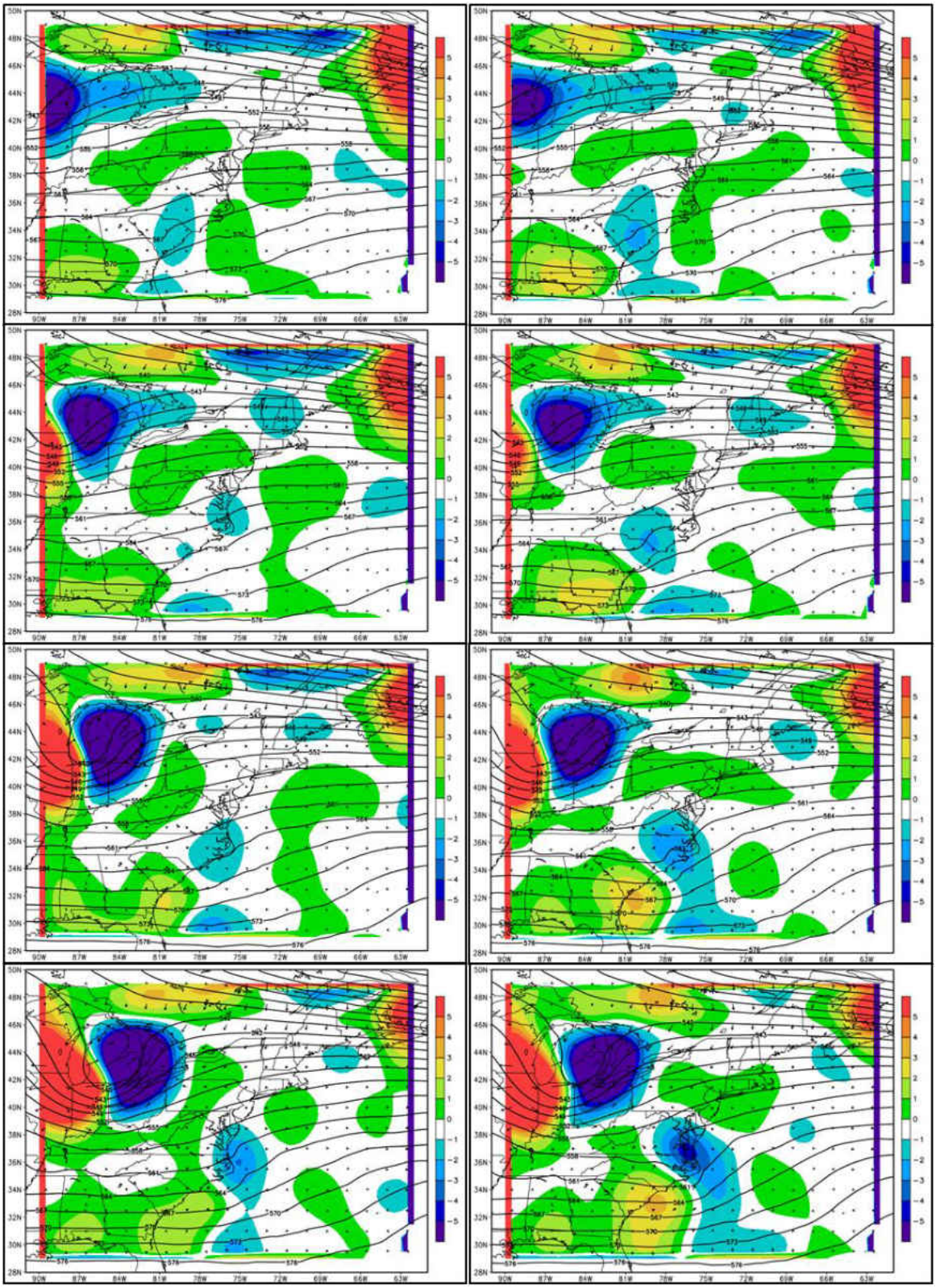

Fig. 14. 0600 UTC (left) and 1200 UTC (right) 7 Feb 2013 NAM forecasts for 500 hPa heights (dam, solid), Q-vectors (arrows in $x10^{-7}$ Pa m^{-1} s^{-1}), and Q-vector divergence (10^{-12} Pa m^{-2} s^{-1}) valid at 0300 UTC, 0600 UTC, 0900 UTC, and 1200 UTC 8 Feb 2013 (top to bottom).

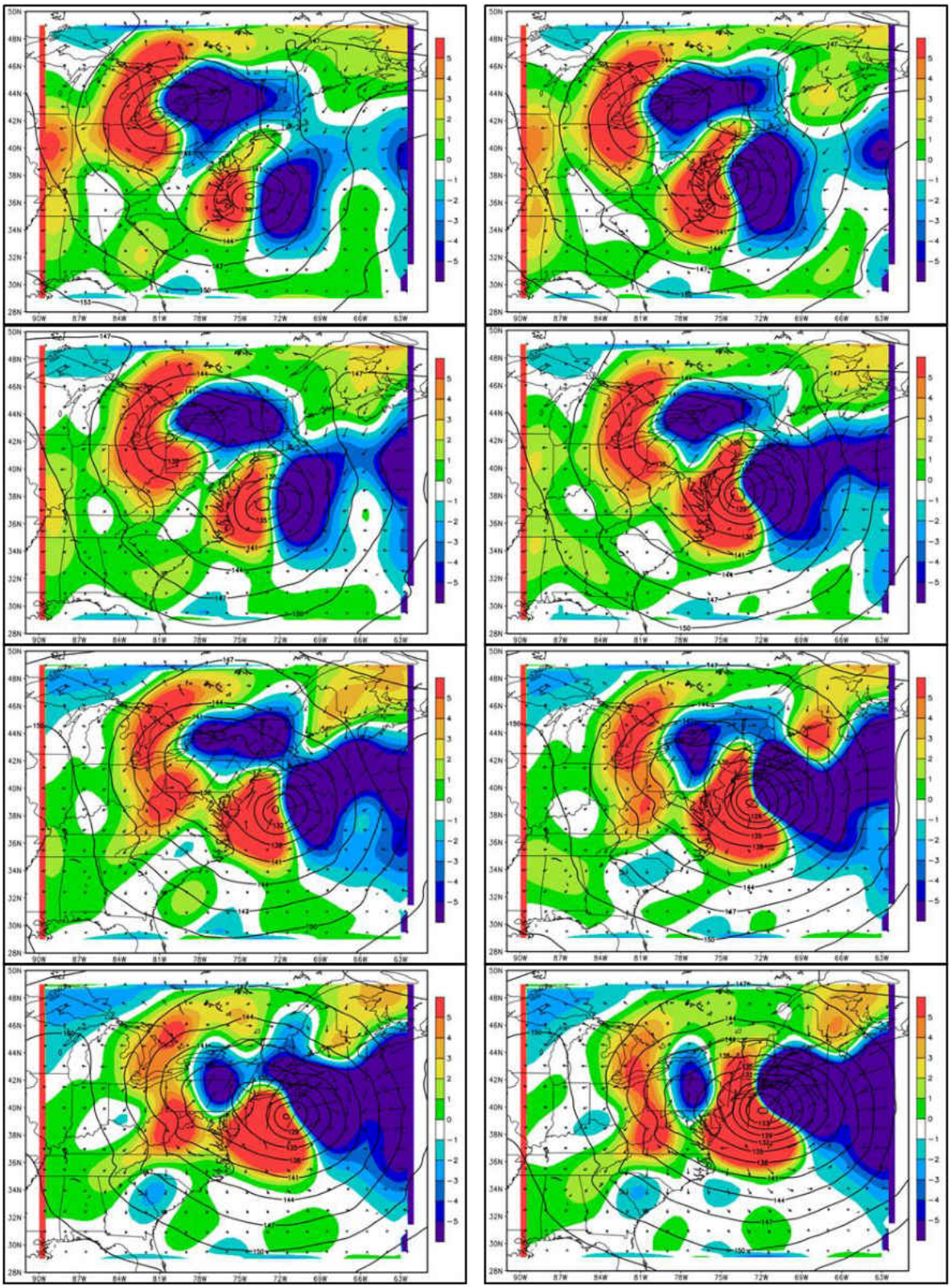

Fig. 15. 0600 UTC (left) and 1200 UTC (right) 7 Feb 2013 NAM forecasts for 850 hPa heights (dam, solid), Q-vectors (arrows in $x10^{-7}$ Pa m^{-1} s^{-1}), and Q-vector divergence (10^{-12} Pa m^{-2} s^{-1}) valid at 1800 UTC and 2100 UTC 8 Feb 2013, 0000 UTC and 0300 UTC 9 Feb 2013 (top to bottom).

When assessing snowband placement, often the focus shifts to analyzing frontogenesis in the presence of CSI. However, the intense reflectivity forecast does not align with the frontogenesis forecast at any of three different levels (1000 hPa, 850 hPa, and 700 hPa). Rather, the frontogenesis, which slopes with height toward the cold air (Novak et al. 2006), remains to the east or southeast of the strongest reflectivity, even at 700 hPa (Fig. 16). There is only one instance in the 0706Z run, the forecast valid at 0000 UTC 9 February, in which the frontogenesis aligns with the reflectivity (Fig. 17). Examining a cross section (Fig. 18) at this time taken perpendicular to the thermal wind of M_g-θ_{es} indicates the presence of CSI, as the θ_{es} lines are more steeply sloped than the M_g lines between 72W and 73W (estimates of the longitudes surrounding the location of the most intense reflectivity).

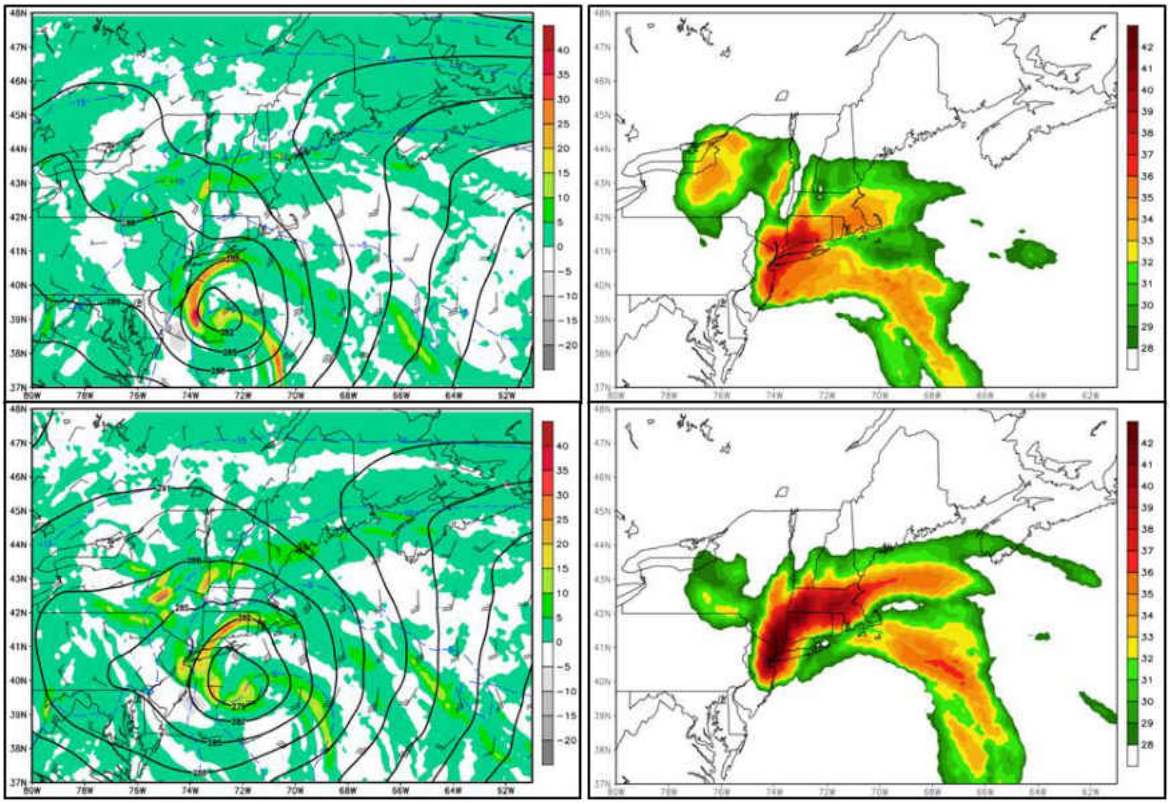

Fig. 16. 1200 UTC 7 Feb 2013 NAM forecast valid at 0000 UTC 9 Feb 2013 (top) and 0300 UTC 9 Feb 2013 (bottom) for 700hPa frontogenesis (C/100km, shaded), height (dam, solid), and wind (m/s, barb) (left); composite reflectivity (dBZ) (right).

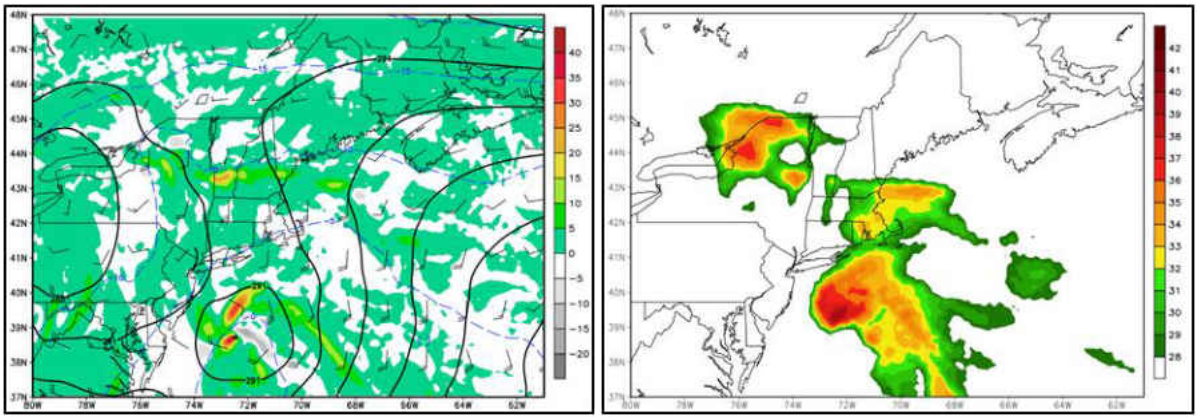

Fig. 17. 0600 UTC 7 Feb 2013 NAM forecast valid at 0000 UTC 9 Feb for 700hPa frontogenesis (C/100km, shaded), height (dam, solid), and wind (m/s, barb) (left); composite reflectivity (dBZ) (right).

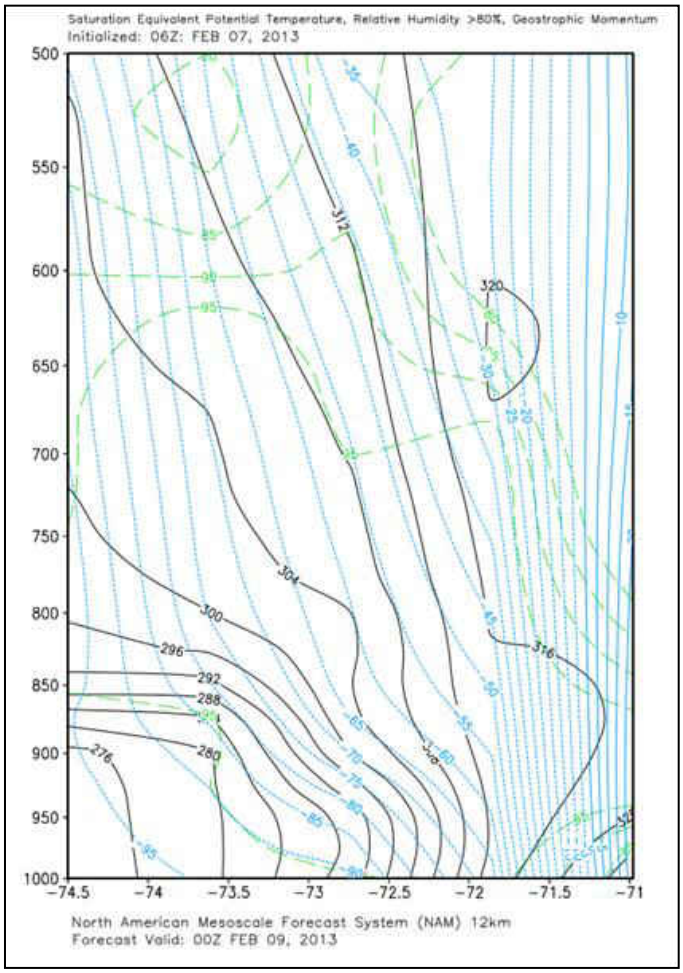

Fig. 18. 0600 UTC 7 Feb 2013 NAM forecast valid at 0000 UTC 9 Feb - Cross section of geostrophic momentum (M_g) (m/s, blue), saturation equivalent potential temperature (θ_{es}) (K, black), and relative humidity >80% (%, green).

In respect to the most intense forecast reflectivity at further times, there is a very small presence of CSI roughly between 825-725 hPa (within 70.7W and 72W) at 0300 UTC 9 February, while there is a stronger presence at 0600 UTC 9 February. However, most of it is found fairly high aloft, higher than 700 hPa. As for the 0712Z run, there are no times in which the forecast mid-level frontogenesis (Fig. 19c) aligns with the forecast reflectivity (Fig. 19a), while CSI also remains absent from the band location. Accordingly, we must conclude that the collocation of CSI with frontogenesis is not the primary reason for band development in these forecasts, but rather that the bands result primarily from the strong and focused WAA pattern (Fig. 19d). Notably, there is also some contribution from differential cyclonic geostrophic vorticity advection (Fig. 19b), which aligns directly or just slightly to the east of the most intense reflectivity. Thus, the combination of WAA and cyclonic vorticity advection appears to be providing the localized areas of intense vertical motion producing these snowbands.

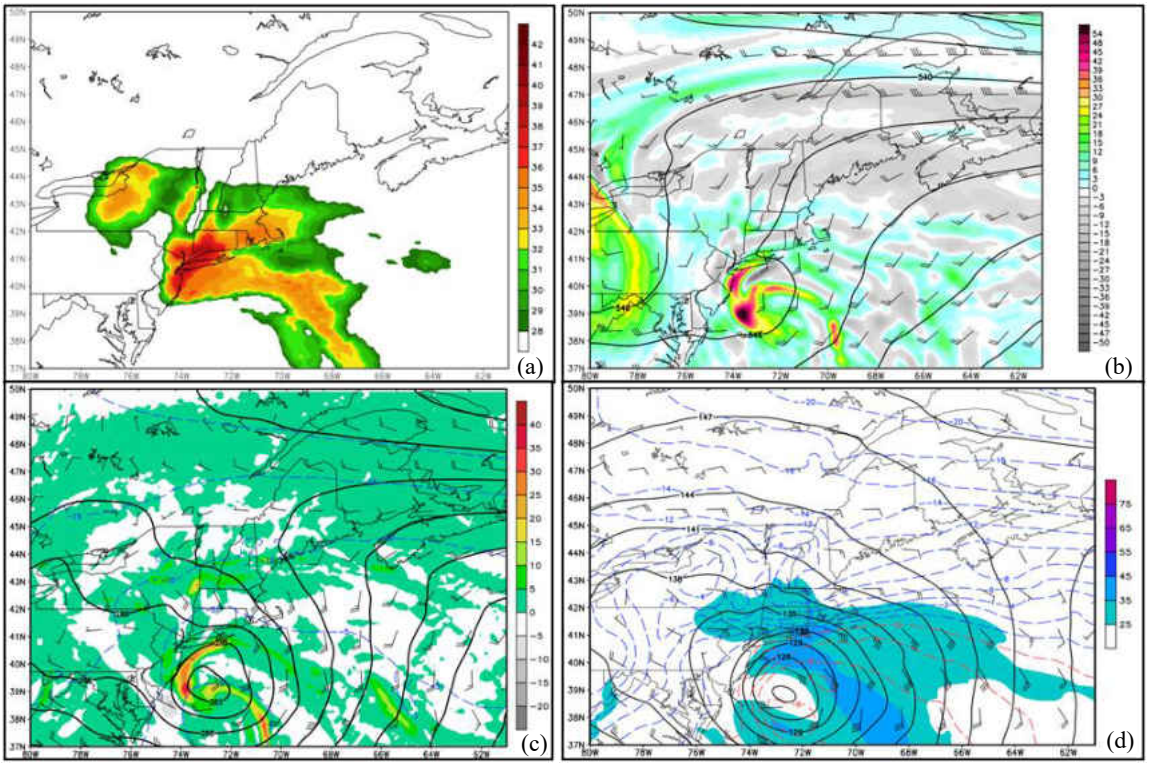

Fig. 19. 1200 UTC 7 Feb 2013 NAM forecast valid at 0000 UTC 9 Feb for (a) composite reflectivity (dBZ); (b) 500 hPa heights (dam, solid), winds (m/s, barb), and vorticity (10^{-5} s^{-1}, shaded); (c) 700hPa frontogenesis (C/100km, shaded), height (dam, solid), and wind (m/s, barb); (d) 850 hPa heights (dam, solid), temperature (C, dashed), and winds (m/s, barb).

c. Forecast Shift between 0000 UTC 8 February and 0600 UTC 8 February

At 500 hPa (Fig. 20), approximately the same pattern occurs for both the 0000 UTC 8 February and the 0600 UTC 8 February runs (hereafter referred to as 0800Z and 0806Z respectively). There is a broad, negatively tilted trough over the East Coast with its axis running through the North Carolina and South Carolina border, while another trough is over the Great Lakes. As time progresses, not many differences occur between the two until 1800 UTC, when the 552 dam contour amplifies over southeastern Maryland within 0800Z. The other run, 0806Z, instead forms a very small closed 552 dam contour over southeastern Maryland. The 500 hPa cyclonic geostrophic vorticity advection in 0800Z is significantly stronger in all of the forecast hours leading up to the valid time for 1800 UTC 8 February. This difference likely is the reason the 0806Z run did not produce the sharp 552 dam contour as compared to 0800Z, which is also consistent with the deepening of cyclone central pressure in 0800Z to 994 hPa off the southeastern coast of Maryland, as opposed to 996 hPa for 0806Z.

Another difference that emerges between these runs is in the location of the surface cyclone, which is consistently farther to the west in 0800Z compared to 0806Z. At the start/analysis time of 0806Z and the matching forecast time within 0800Z, it is evident that the 850 hPa heights are slightly lower in 0800Z, with a closed contour of 141 dam over eastern South Carolina compared to a broad 144 dam contour stretching across a majority of the eastern Carolinas in 0806Z (Fig. 21). Since 0806Z is the analysis time, 0800Z already shows a slight forecast error. The evolution of this error can be seen through the 850 hPa Q-Vector analysis (Fig. 22), which shows that the convergence/divergence couplet in 0800Z is tighter, more intense, and shifted slightly to the west by 0600 UTC 8 February. Throughout the rest of the run this remains the case, as Sutcliffe self-development continues to strengthen the cyclone, while

tracking it to the north/northeast compared to 0806Z (Fig. 23). Thus, the associated deep surface cyclone tracks closer to the coast, and the reflectivity develops farther to the west (Fig. 23a). In contrast, the strongest frontogenetical forcing (Figs. 23c,g) remains slightly to the east or southeast throughout the runs, confirming the lesser importance of frontogenetical processes to the positioning of the bands.

Also, for valid times of 0000 UTC, 0300 UTC, 0600 UTC, there was no indication of CSI occurring within the banded regions, with exception to some found high aloft at 0000 UTC (around 625 hPa and above). However, outside of the intense banded regions, there is some CSI to the northwest of the main bands found nearer to the mid-levels which coincides with weaker forecast reflectivities. In particular 0800Z valid at 0300 UTC has CSI roughly aligning with both weak reflectivity and weak mid-level frontogenesis over west-central portions of New York (Figs. 24a-c), while 0806Z valid at 0300 UTC depicts only CSI corresponding with weaker reflectivity over eastern New York (Figs. 24d-f). Regardless, our area of focus with the main reflectivity bands is lacking the presence of both mesoscale parameters, verifying that quasigeostrophic forces of strong WAA and some cyclonic vorticity advection are of greater cause for the band development and placement within this case.

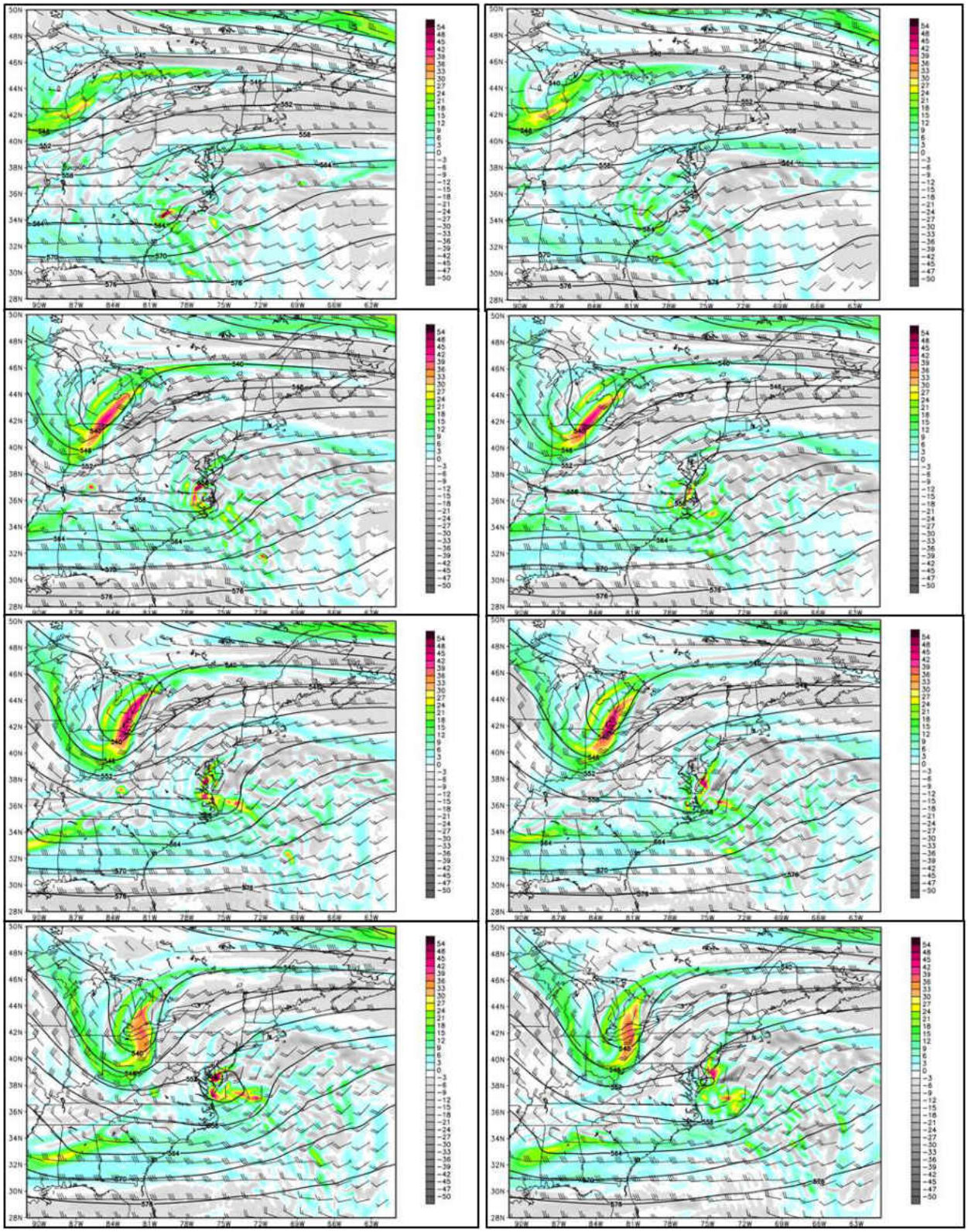

Fig. 20. 0000 UTC (left) and 0600 UTC (right) 8 Feb 2013 NAM forecasts for 500 hPa heights (dam, solid), winds (m/s, barb), and vorticity (10^{-5} s^{-1}, shaded) valid at 0600 UTC, 1200 UTC, 1500 UTC, and 1800 UTC 8 Feb 2013 (top to bottom).

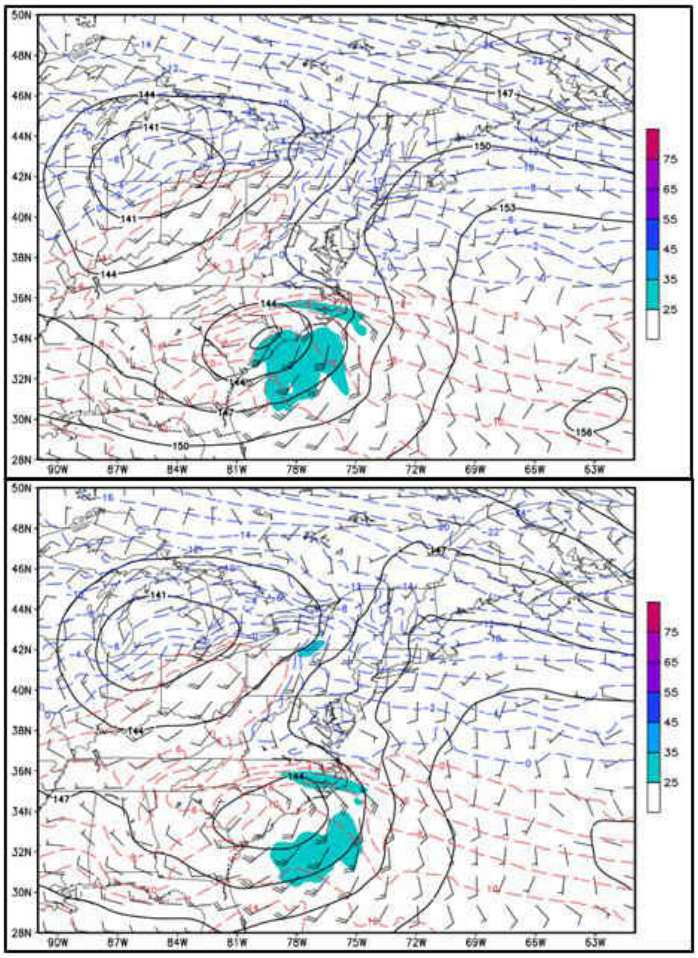

Fig. 21. 0000 UTC (top) and 0600 UTC (bottom) 8 Feb 2013 NAM forecasts for 850 hPa heights (dam, solid), temperature (C, dashed), and winds (m/s, barb) valid 0600 UTC 8 Feb 2013 (top) and 0000 UTC 8 Feb 2013 (bottom).

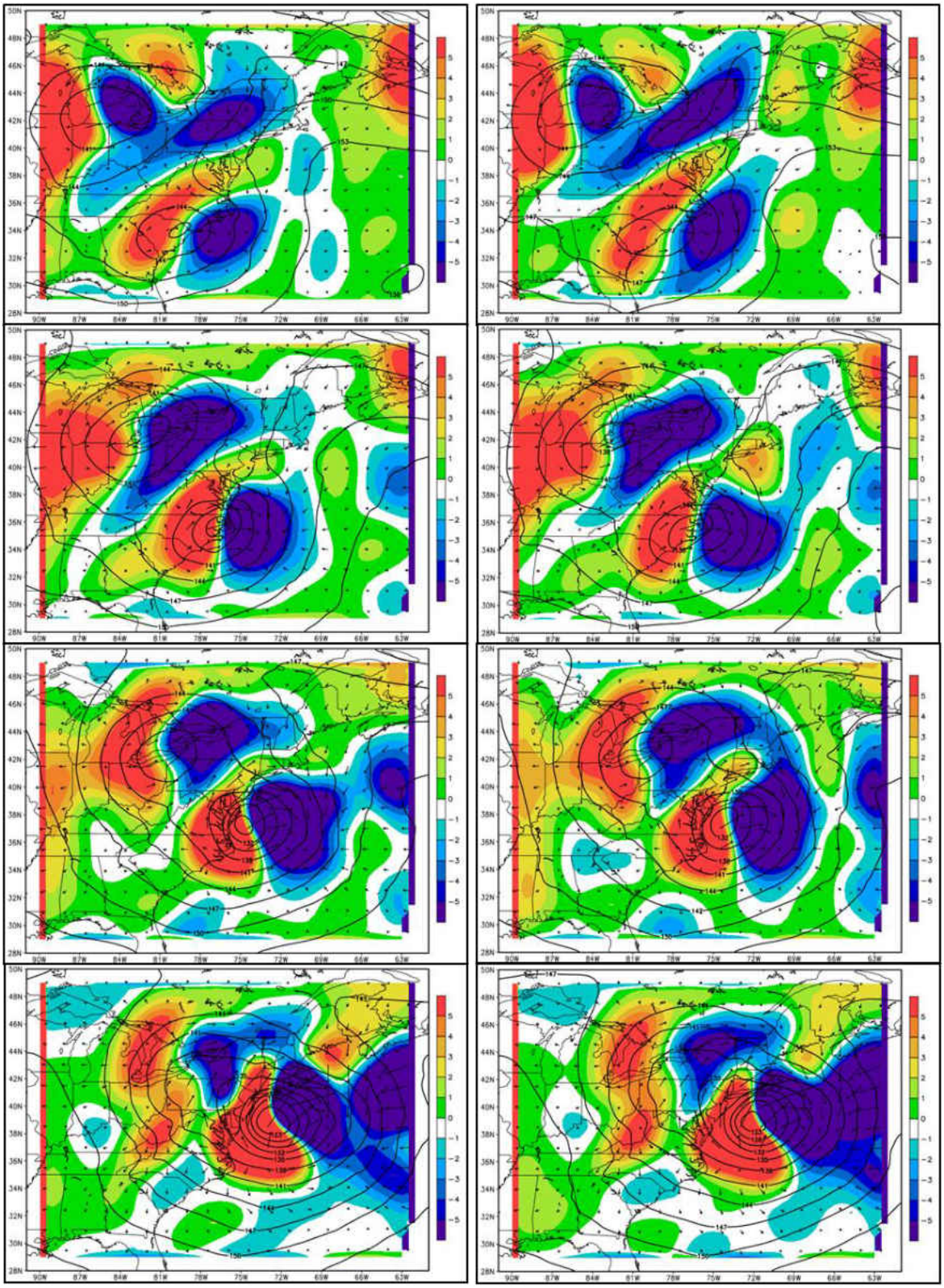

Fig. 22. 0000 UTC (left) and 0600 UTC (right) 8 Feb 2013 NAM forecasts for 850 hPa heights (dam, solid), Q-vectors (arrows in $x10^{-7}$ Pa m^{-1} s^{-1}), and Q-vector divergence (10^{-12} Pa m^{-2} s^{-1}) valid at 0600 UTC, 1200 UTC, 1800 UTC 8 Feb 2013 and 0000 UTC 9 Feb 2013 (top to bottom).

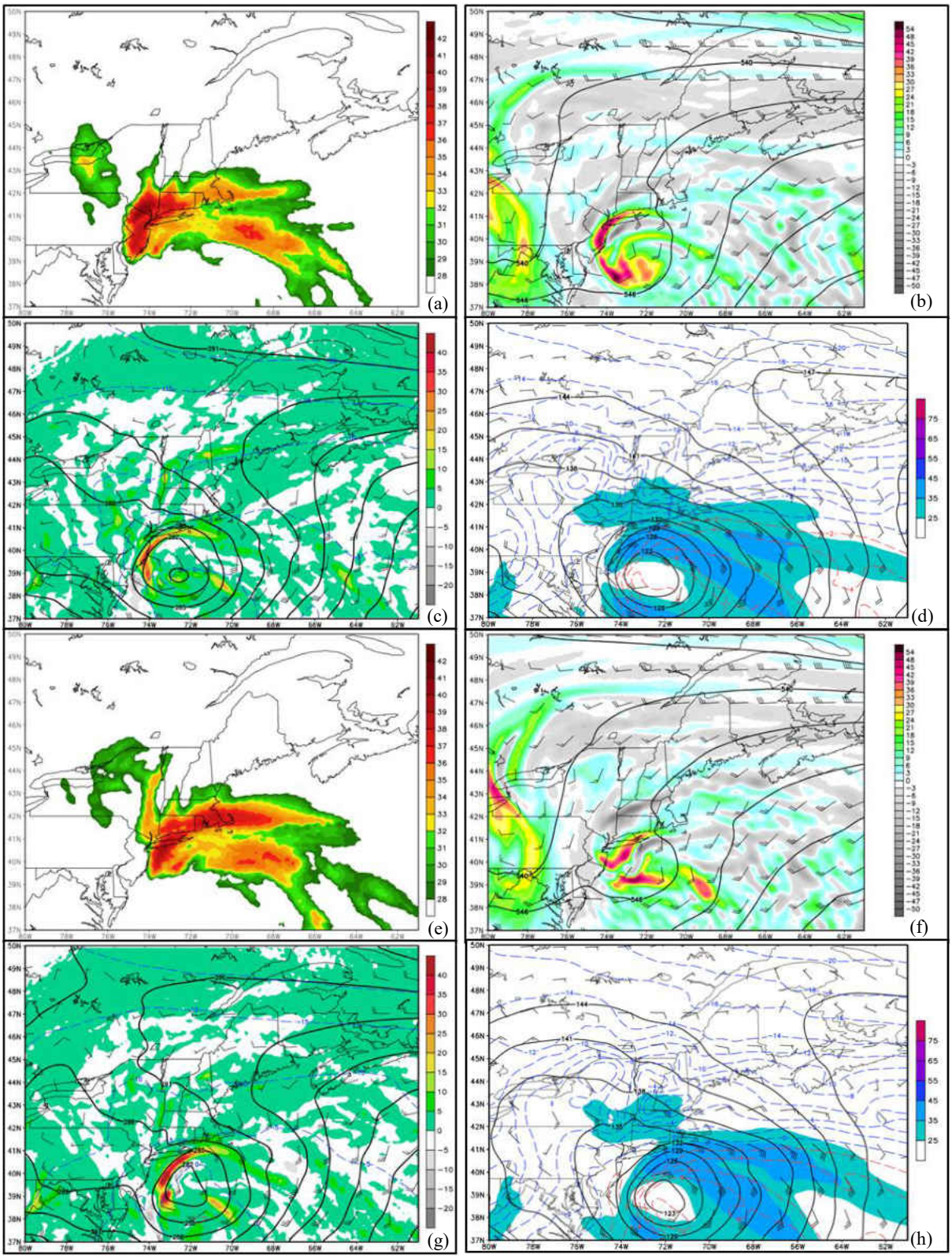

Fig. 23. 0000 UTC 8 Feb 2013 NAM forecast valid at 0000 UTC 9 Feb 2013 for (a) composite reflectivity (dBZ); (b) 500 hPa heights (dam, solid), winds (m/s, barb), and vorticity (10^{-5} s^{-1}, shaded); (c) 700hPa frontogenesis (C/100km, shaded), height (dam, solid), and wind (m/s, barb); (d) 850 hPa heights (dam, solid), temperature (C, dashed), and winds (m/s, barb). Same for (e-h) but for 0600 UTC 8 Feb 2013 forecast valid at 0000 UTC 9 Feb 2013.

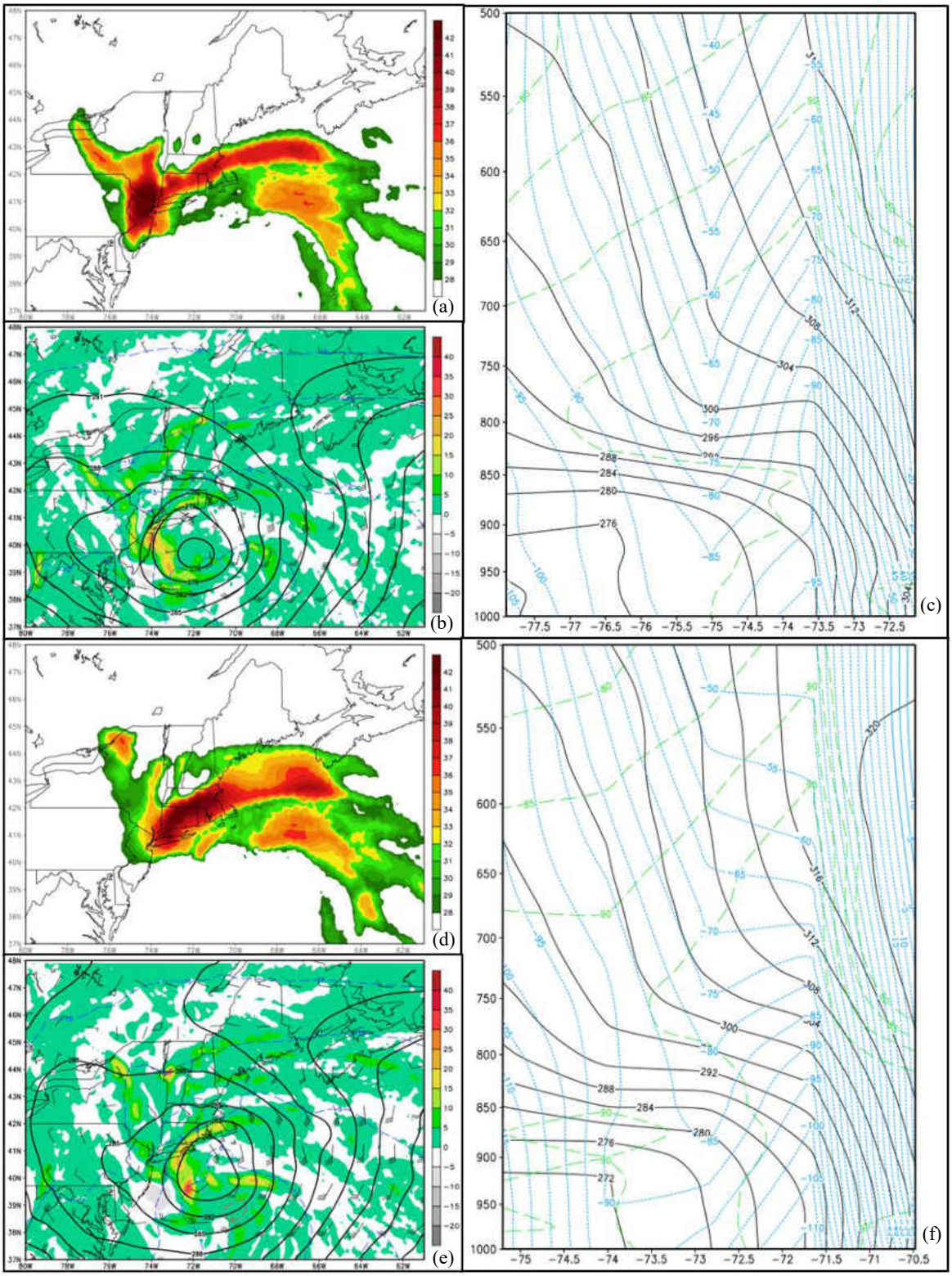

Fig. 24. 0000 UTC 8 Feb 2013 NAM forecast valid at 0300 UTC 9 Feb 2013 for (a) composite reflectivity (dBZ); (b) 700hPa frontogenesis (C/100km, shaded), height (dam, solid), and wind (m/s, barb); (c) cross section of geostrophic momentum (M_g) (m/s, blue), saturation equivalent potential temperature (θ_{es}) (K, black), and relative humidity >80% (%, green); same for (d-f) but for 0600 UTC 8 Feb 2013 NAM forecast valid at 0300 UTC 9 Feb 2013.

IV. DISCUSSION

NAM forecasts leading up to the strong extratropical cyclone event of 8-9 February 2013 were investigated on a run-to-run basis to better understand the variability that occurred amongst them with respect to snowband placement. More specifically, the evolution of the synoptic patterns was assessed using quasigeostrophic theory, with Q-Vector analyses helping to focus areas in which differential vorticity advection and the Laplacian of warm air advection were prominent. To assess the development of the banded precipitation, mid-level total wind frontogenesis was also calculated and diagnosed in concert with the M_g-θ_{es} technique used to evaluate the presence of CSI. It was discovered that for this particular event, the collocation of these two factors, mid-level frontogenesis and CSI, were not strongly tied to the production of the precipitation. The frontogenesis consistently stayed to the east or southeast of the banded precipitation, while CSI was scarcely present within the atmosphere at the valid times of 0000 UTC, 0300 UTC, and 0600 UTC 9 February 2013.

However, it is important to note that the M_g-θ_{es} cross-section technique, used to ascertain susceptibility to slantwise displacements within the atmosphere, is not the most preferred method given certain required assumptions. These requirements are (1) the geostrophic wind should be constant in the alongfront direction; (2) the cross section for evaluating the M_g-θ_{es} relationship should be perpendicular to the thermal wind; and (3) the ageostrophic wind should be small (Schultz and Schumacher 1999). For this study, the first two criteria were met; however, the third criteria may be problematic in certain locations and times, given the relatively strong flow curvature associated with a maturing extratropical cyclone. However, the specific times at which CSI was identified with forecast banding occurred in places where the gradient was relatively weak and/or the flow was straight and as such, the ageostrophic flow was resultantly small. For

increased confidence, however, it would be useful to compare this assessment to one obtained through calculation of moist potential vorticity (MPV), specifically that of saturated equivalent geostrophic potential vorticity (Schultz and Schumacher 1999), since that approach is not subject to the same M_g-θ_{es} sectional constraints.

Nonetheless, it is apparent that the frontogenesis and CSI does not align well with the forecast reflectivity, especially since the former is most often shifted to the east or southeast. Therefore, these ingredients, which are commonly attributed to mesoscale snowband development within the "comma head" portion of the cyclone (Novak 2004), were not found to be significant contributors to this *high-impact* case. Instead, the band placement and development was primarily a result of strong quasigeostrophic dynamics, particularly that of strong and focused WAA, along with some contribution from differential cyclonic geostrophic vorticity advection that appeared directly or just slightly to the east of the most intense reflectivity. Further, the time-integrated WAA was largely responsible for variations in the cyclone track which alternatively brought the attendant snowbands directly over or to the east of the NYC area.

From an operational perspective, this study emphasizes the importance of carefully diagnosing the evolution of the synoptic patterns associated with an extratropical cyclone, as the details regarding banded development could be largely attributed to the quasigeostrophic dynamics instead of the typical mesoscale ingredients referred to in most snowband research. Also, this study is consistent with the findings of Evans and Jurewicz (2009) in that timing and location of forecast intense snowband signatures are unreliable more than twelve hours out. Here, there were two large shifts, primarily driven by the placement of WAA that occurred within the NAM forecasts leading up to this event. The first one between 0706Z and 0712Z was approximately 42 hours and 36 hours out respectively from when observations of intense banded

precipitation transpired, with the second shift noted between 0800Z and 0806Z (24 hours and 18 hours out respectively). Forecasting a high-impact snowstorm is a complex task which necessarily involves assessing a variety of factors that contribute to the evolution of the parent storm and its attendant precipitation, and combining that information into a coherent and physically consistent vision of the event. Although we have not undertaken an analysis of the actual forecasts issued by Weather Service Offices or the NOAA's Weather Prediction Center, this case presents a cautionary tale of what could happen if forecasters focus their attention too much on the well-known factors to the exclusion of others.

REFERENCES

Evans, M., and M. L. Jurewicz Sr., 2009: Correlations between analyses and forecasts of banded heavy snow ingredients and observed snowfall. *Wea. Forecasting*, **24,** 337–350.

Gaza, R. S., and L. F. Bosart, 1990: Trough merger characteristics over North America. *Wea. Forecasting*, **5**, 314–331.

Jurewicz, M. L., and M. S. Evans, 2004: A comparison of two banded heavy snowstorms with very different synoptic settings. *Wea. Forecasting*, **19**, 1011–1028.

Nicosia, D. J., and R. H. Grumm, 1999: Mesoscale band formation in three major northeastern United States snowstorms. *Wea. Forecasting*, **14,** 346–368.

Novak, D. R., L. F. Bosart, D. Keyser, and J. S. Waldstreicher, 2004: An observational study of cold season-banded precipitation in northeast U.S. cyclones. *Wea. Forecasting*, **19,** 993-1010.

Novak, D. R., J. S. Waldstreicher, D. Keyser, and L. F. Bosart, 2006: A forecast strategy for anticipating cold season mesoscale band formation within eastern U.S. cyclones. *Wea. Forecasting*, **21**, 3–23.

Novak, D. R., B. A. Colle, and A. Aiyyer, 2010: Evolution of mesoscale precipitation band environments within the comma head of northeast U.S. cyclones. *Mon. Wea. Rev.*, **138**, 2354–2374.

Novak, D. R., and B. A. Colle, 2012: Diagnosing snowband predictability using a multimodel ensemble system. *Wea. Forecasting*, **27**, 565–585.

NWA, cited 2016: Update on the February 8-9 2013 nor'easter/southern New England blizzard. National Weather Association. [Available online at http://www.nwas.org/archive/2013/WinterStorms2013.]

Palmén, E., and C. W. Newton, 1969: *Atmospheric Circulation Systems*. Academic Press, 603 pp.

Picca, J. C., D. M. Schultz, B. A. Colle, S. Ganetis, D. R. Novak, and M. J. Sienkiewicz, 2014: The value of dual-polarization radar in diagnosing the complex microphysical evolution of an intense snowband. *Bull. Amer. Meteor. Soc.*, **95**, 1825-1834.

Schultz, D. M., and P. N. Schumacher, 1999: The use and misuse of conditional symmetric instability. *Mon. Wea. Rev.*, **127**, 2709–2732; Corrigendum, 128, 1573.

Sutcliffe, R. C., and A. G. Forsdyke, 1950: The theory and use of upper air thickness patterns in forecasting. *Quart. J. Roy. Meteor. Soc.*, **76**, 189-217.

Uccellini, L. W., 1990: Processes contributing to the rapid development of extratropical cyclones. *Extratropical Cyclone: The Erik Palmén Memorial Volume*, C. W. Newton and E. O. Holopainen, Eds., *Amer. Meteor. Soc.*, 81-105.

NAM Configuration Link:
http://www.emc.ncep.noaa.gov/mmb/mmbpll/misc/nam_2014_specs/index.html